Multilayer shallow water equations with complete Coriolis force. Part 3. Hyperbolicity and stability under shear

Andrew L. Stewart† and Paul J. Dellar

OCIAM, Mathematical Institute, University of Oxford, 24-29 St Giles', Oxford, OX1 3LB, UK

(Received 19 April 2012, revised 23 December 2012, accepted 4 February 2013)

We analyse the hyperbolicity of our multilayer shallow water equations that include the complete Coriolis force due to the Earth's rotation. Shallow water theory represents flows in which the vertical shear is concentrated into vortex sheets between layers of uniform velocity. Such configurations are subject to Kelvin–Helmholtz instabilities, with arbitrarily large growth rates for sufficiently short wavelength disturbances. These instabilities manifest themselves through a loss of hyperbolicity in the shallow water equations, rendering them ill-posed for the solution of initial value problems. We show that, in the limit of vanishingly small density difference between the two layers, our two-layer shallow water equations remain hyperbolic when the velocity difference remains below the same threshold that also ensures the hyperbolicity of the standard shallow water equations. Direct calculation of the domain of hyperbolicity becomes much less tractable for three or more layers, so we demonstrate numerically that the threshold for the velocity differences, below which the three-layer equations remain hyperbolic, is also unchanged by the inclusion of the complete Coriolis force. In all cases, the shape of the domain of hyperbolicity, which extends outside the threshold, changes considerably. The standard shallow water equations only lose hyperbolicity due to shear parallel to the direction of wave propagation, but the complete Coriolis force introduces another mechanism for loss of hyperbolicity due to shear in the perpendicular direction. We demonstrate that this additional mechanism corresponds to the onset of a transverse shear instability driven by the non-traditional components of the Coriolis force in a three-dimensional continuously stratified fluid.

1. Introduction

Systems of shallow water and shallow water-like equations enjoy widespread use as both conceptual and predictive models in geophysical fluid dynamics (Pedlosky 1987; Salmon 1998; Vallis 2006). Owing to their simplified two-dimensional description of three-dimensional processes with large horizontal length scales, shallow water models have been applied to a diverse range of oceanographic and atmospheric phenomena. They have contributed fundamentally to our understanding of mesoscale processes such as baroclinic instability (*e.g.* Phillips 1954; Boss, Paldor & Thompson 1996; Vallis 2006) and internal waves (*e.g.* LeBlond & Mysak 1978). They have been used to describe the interaction between the surface mixed layer and the deep ocean (*e.g.* LeBlond & Mysak 1978; Salmon 1982), the dynamics of the troposphere and stratosphere (*e.g.* Vallis 2006), and the flow of abyssal currents over rough bottom topography (*e.g.* Stephens & Marshall 2000; Choboter & Swaters 2004; Marchal & Nycander 2004). They also form the basis of the Lagrangian vertical discretisations used in several predictive ocean general circulation models such as the Miami Isopycnic Coordinate Ocean Model (MICOM, Bleck *et al.* 1992; Bleck & Chassignet 1994) and the Generalized Ocean Layered Model (GOLD, Adcroft & Hallberg 2006).

Large-scale atmospheric and oceanic flows are dominated by the Coriolis force due to the Earth's rotation. However, standard shallow water theory retains only the components of the Coriolis force due to the locally vertical component of the Earth's rotation vector. This approximation was named the traditional approximation by Eckart (1960), on the grounds that its widespread use was driven more by technical convenience, such as allowing separable normal modes, than by theoretical justification. In more recent work, the traditional approximation is commonly assumed to be valid when the ratio of vertical to horizontal length scales is small (Gerkema *et al.* 2008), or when the fluid is strongly stratified so that the buoyancy or Brunt–Väisälä frequency N is much larger than the inertial frequency (Queney 1950; Phillips 1968, 1973; Thuburn *et al.* 2002). The neglected "non-traditional" components of the Coriolis force, proportional to the locally horizontal component of the rotation vector, may have a pronounced effect in weakly-stratified regions of the oceans. These include the deep Mediterranean (van Haren & Millot 2005), the Southern Ocean with $N = (5.4 \pm 0.2) \times 10^{-4}\,\mathrm{s}^{-1}$ (Heywood *et al.* 2002), and the Labrador Sea with $N \sim 2.1 \times 10^{-4}\,\mathrm{s}^{-1}$ (Lazier 1980). Gerkema *et al.* (2008) recently reviewed a range of oceanographic and atmospheric phenomena that are substantially influenced by non-traditional effects, such as Ekman spirals (*e.g.* Leibovich & Lele 1985), deep convection (*e.g.* Marshall & Schott 1999), and internal waves (*e.g.* Gerkema & Shrira 2005*a*,*b*; Stewart & Dellar 2012*b*).

Dellar & Salmon (2005) derived one-layer shallow water equations that include the complete Coriolis force. Stewart &

† Now at: Environmental Science and Engineering, California Institute of Technology, Pasadena, CA 91125, USA. Email addresses: stewart@gps.caltech.edu and dellar@maths.ox.ac.uk.

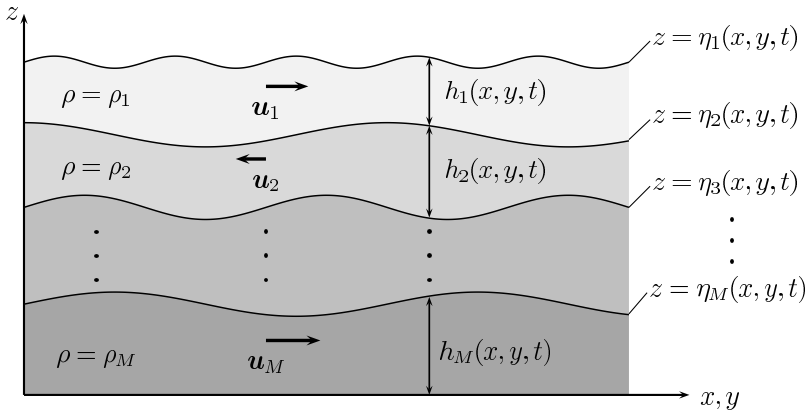

FIGURE 1. A schematic of the multilayer shallow water model showing the horizontal velocities $\boldsymbol{u}_i$ within the layers.

Dellar (2010) extended this derivation to arbitrarily many layers, as illustrated in figure 1. These equations provide a tractable reduced description that includes non-traditional effects, aiding our understanding of some of the phenomena surveyed by Gerkema *et al.* (2008). For example, Stewart & Dellar (2012*b*) showed that the non-traditional components of the Coriolis force substantially modifies long linear plane waves, a surprising result given that the traditional approximation is commonly believed to hold particularly well for long waves with their small aspect ratios. This modification arises from a distinguished limit in which the up- and down-wellings driven by non-traditional Coriolis terms become comparable to the horizontal pressure gradient for sufficiently long waves. Stewart & Dellar (2011*a*,*b*, 2012*a*) demonstrated that the interaction of the complete Coriolis force with bottom topography may substantially enhance the cross-equatorial flow of abyssal ocean currents, such as the Antarctic Bottom Water, due to a partial cancellation between a non-traditional topographic contribution to the potential vorticity and the variation with latitude of the planetary contribution.

In this paper we investigate the domain of hyperbolicity of the multilayer shallow water equations with complete Coriolis force. Multilayer shallow water theory represents flows in which vertical changes in the horizontal velocity are concentrated into vortex sheets between layers of uniform velocity, as illustrated in figure 1. Such flows are subject to Kelvin–Helmholtz instabilities. These instabilities are suppressed at large length scales by stabilising density contrasts between layers, but sufficiently short length scales always remain unstable, with growth rates that increase proportionally to the wave number k of the disturbance (Taylor 1931; Goldstein 1931; Lamb 1932, §232; Chandrasekhar 1961, §101). The appearance of growth rates proportional to k in the Kelvin–Helmholtz instability establishes the *ill-posedness* of the initial value problem for both the shallow water and the three-dimensional equations. The description "ill-posed" refers to the impossibility of bounding the amplitude of the disturbance at some time $t > 0$ by a fixed multiple of the amplitude of the disturbance at $t = 0$ in the same norm (Hadamard 1923; Joseph & Saut 1990; Renardy & Rogers 2004). Mathematically, the ill-posedness appears as a loss of hyperbolicity of the shallow water equations, which instead become elliptic. Elliptic equations offer the canonical examples of ill-posed initial value problems. The hyperbolicity condition in one spatial dimension corresponds to small disturbances propagating along real characteristic curves in the space-time plane, while the generalisation to characteristic surfaces in multiple spatial dimensions is given in §3 below. Establishing the hyperbolicity of our equations therefore serves as an important test to establish their range of validity for solving initial value problems. More recently, Chumakova *et al.* (2009*a*,*b*) highlighted the connection between many familiar fluid instability conditions, such as the Miles–Howard condition (Miles 1961; Howard 1961) for instability of stratified shear flows, and the loss of well-posedness of either the layered or the continuously stratified fluid equations.

Standard shallow water theory is based on the hydrostatic approximation, which neglects inertia in the vertical momentum equation. This tames the Kelvin–Helmholtz instability of vortex sheets, to the extent that it may be completely suppressed by sufficiently strong stratification (Long 1956; Kelder & Teitelbaum 1991). For example, Long (1956) showed that the two-layer shallow water equations with a rigid lid are hyperbolic when the velocity difference between the two layers is less than a threshold $(g'H)^{1/2}$ set by the reduced gravity g' and the total depth H of the two layers. Houghton & Isaacson (1970) showed that the two-layer shallow water equations with a free surface are hyperbolic when the velocity difference is less than twice the internal wave speed (see §4.2). Liska & Wendroff (1997) summarised these results, and showed that the multilayer extensions of the Green & Naghdi (1976) equations, which retain the vertical acceleration whilst preserving the assumption of columnar motion, are unconditionally ill-posed even for arbitrarily small (but nonzero) velocity differences between adjacent layers.

The above results all apply in the absence of rotation. Rotation about a vertical axis leaves the hydrostatic approximation unmodified, and also leaves the hyperbolicity conditions for the multilayer shallow water equations unmodified. Mathematically, this is because the traditional Coriolis terms appear as undifferentiated algebraic terms in the shallow water equations, while the hyperbolicity is determined only by the highest derivative terms, the so-called principal part of the symbol (*e.g.*

Joseph & Saut 1990; Renardy & Rogers 2004). By contrast, our shallow water equations are based on the quasihydrostatic approximation introduced by White & Bromley (1995) that includes non-traditional Coriolis terms in the vertical momentum equation, while still neglecting the vertical acceleration.

The structure of this paper is as follows. In §2 and §3 we briefly introduce the multilayer shallow water equations with complete Coriolis force and the hyperbolicity criterion for systems of first-order partial differential equations. In §4 we analyse the hyperbolicity of the two-layer non-traditional shallow water equations in the limit of vanishingly small density difference between the layers. In §5 we present an equivalent numerical study for the three-layer equations, for which the analysis would be considerably more complicated. In §6 we identify the loss of hyperbolicity due to transverse shear in our non-traditional multilayer shallow water equations with a shear instability in the continuously stratified equations driven by the non-traditional components of the Coriolis force. Finally, in §7 we discuss our results and their implication for future studies.

2. The multilayer shallow water equations with complete Coriolis force

This paper is principally concerned with multilayer shallow water equations that include the complete Coriolis force, as derived by Stewart & Dellar (2010). We formulate our equations using the non-traditional version of an f-plane, a pseudo-Cartesian coordinate system that describes a small region of the Earth's surface close to a specific latitude ϕ_0 and longitude λ_0 (*e.g.* Vallis 2006; White 2002; Salmon 1998; Pedlosky 1987; Gill 1982). We align the z-axis normal to surfaces of constant geopotential, with x and y coordinates measuring distance along these surfaces from the point (λ_0, ϕ_0). For analytical convenience we allow arbitrary orientation of the x and y axes, defining θ as the positive angle from East to the x-axis. In these coordinates, the Earth's rotation vector has three non-zero components,

$$\tilde{\Omega}_x = \tilde{\Omega}\cos\phi\sin\theta, \quad \tilde{\Omega}_y = \tilde{\Omega}\cos\phi\cos\theta, \quad \tilde{\Omega}_z = \tilde{\Omega}\sin\phi. \tag{2.1}$$

The tildes ($\tilde{}$) indicate that these are dimensional quantities. We assume that the horizontal scales of motion are much smaller than the Earth's radius, so we neglect spatial variations of the components of $\boldsymbol{\Omega}$ and the curvature of the geopotential surfaces.

The multilayer shallow water equations describe the evolution of superposed layers of incompressible fluid, each with constant density ρ_i, as sketched in figure 1. The fluid in each layer is constrained to move in columns aligned with the locally vertical axis. The depth-averaged horizontal velocity in the i^{th} layer is $\tilde{\boldsymbol{u}}_i = (\tilde{u}_i(x,y,t), \tilde{v}_i(x,y,t))$, and the layer thickness is $\tilde{h}_i(x,y,t)$. The governing equations express conservation of mass,

$$\frac{\partial h_i}{\partial t} + \nabla\cdot(h_i\boldsymbol{u}_i) = 0, \tag{2.2}$$

and of depth-averaged horizontal momentum,

$$\begin{aligned}&\frac{\partial \boldsymbol{u}_i}{\partial t} + (\boldsymbol{u}_i\cdot\nabla)\boldsymbol{u}_i + (\Omega_z - \varepsilon\boldsymbol{\Omega}\cdot\nabla\overline{z}_i)\,\hat{\boldsymbol{z}}\times\boldsymbol{u}_i + \varepsilon\boldsymbol{\Omega}\times\hat{\boldsymbol{z}}\,\frac{\partial\overline{z}_i}{\partial t}\\ &+\nabla\left\{\eta_i + \tfrac{1}{2}\varepsilon h_i(v_i\Omega_x - u_i\Omega_y) + \frac{1}{\rho_i}\sum_{j=1}^{i-1}\rho_j h_j\left(1+\varepsilon\left(v_j\Omega_x - u_j\Omega_y\right)\right)\right\} = 0,\end{aligned} \tag{2.3}$$

within each layer. These equations are written using the dimensionless variables

$$\boldsymbol{x} = \frac{\tilde{\boldsymbol{x}}}{R_{\text{d}}}, \quad t = 2\Omega\tilde{t}, \quad \boldsymbol{u}_i = \frac{\tilde{\boldsymbol{u}}_i}{c}, \quad h_i = \frac{\tilde{h}_i}{H}, \quad \overline{z}_i = \frac{(\eta_i+\eta_{i+1})}{2H}. \tag{2.4}$$

We have non-dimensionalised vertical distances using a typical layer depth H, velocities using the surface gravity wave speed $c = \sqrt{gH}$, and horizontal distances using the external Rossby deformation radius $R_{\text{d}} = c/(2\tilde{\Omega})$ defined using the magnitude $\tilde{\Omega}$ of the rotation vector, not the locally vertical component $\tilde{\Omega}_z$. The $\overline{z}_i$ are the vertical coordinates of the mid-surfaces of each layer, equal to the average of z over the i^{th} layer. The ratio of vertical to horizontal length scales,

$$\varepsilon = H/R_{\text{d}} = 2\tilde{\Omega}\sqrt{H/g} = 2\tilde{\Omega}H/c, \tag{2.5}$$

measures the importance of the non-traditional component of the Coriolis force. It also gives the ratio between the horizontal wave speed c and the zonal velocity $\tilde{\Omega}H$ gained or lost by an angular-momentum-conserving displacement of a particle vertically by distance H (White & Bromley 1995). The traditional approximation corresponds to setting $\varepsilon = 0$, thereby neglecting the horizontal components Ω_x and Ω_y of the rotation vector. The specimen parameters $g = 9.81\,\text{m}\,\text{s}^{-1}$, $\tilde{\Omega} = 7.29\times10^{-5}\,\text{rad}\,\text{s}^{-1}$ and $H = 1000\,\text{m}$ give a very small aspect ratio $\varepsilon \approx 1.5\times10^{-3}$. However, we should replace g with a reduced gravity $g' = g\Delta\rho/\rho$ when studying internal waves, since since $\sqrt{g'H}$ is the relevant velocity scale. Since $\Delta\rho/\rho$ may be as small as 10^{-4} for the deep ocean, the relevant aspect ratio ε' may be two to four orders of magnitude larger than the ε defined in (2.5).

3. Requirements for hyperbolicity

In the three-dimensional Euler equations a vortex sheet, an interface across which the tangential velocity is discontinuous, is subject to a Kelvin–Helmholtz instability whose growth rate is proportional to the wave number k of the disturbance. The shallow water equations are founded on the assumption of approximately columnar motion, and so cannot describe the rolling-up of interfaces under the Kelvin–Helmholtz instability. Instead, the shallow water equations lose their hyperbolicity, becoming elliptic, and thus ill-posed for the solution of initial value problems.

The non-rotating multilayer shallow water equations, as derived using the hydrostatic approximation, typically remain hyperbolic as long as the velocity difference between adjacent layers remains sufficiently small compared with the speed of internal waves (*e.g.* Long 1956; Lawrence 1990; Liska *et al.* 1995; Liska & Wendroff 1997). This serves as a measure of the strength of the stable stratification. Including rotation under the traditional approximation, *i.e.* about a vertical axis, has no effect on the hyperbolicity of shallow water models, as described below. Including the complete Coriolis force makes the single-layer shallow water equations ill-posed when the Eastward velocity is very large (Dellar & Salmon 2005). Under these conditions the vertical component of the Coriolis acceleration exceeds the downward acceleration due to gravity, an extreme example of the so-called Eötvös effect (*e.g.* Persson 2005). We expect that the multilayer equations should exhibit some combination of these features. In the following we describe a loss of hyperbolicity as ill-posedness. Strang (1966) has shown that the hyperbolicity conditions we derive below are necessary for well-posedness of the nonlinear system, and elliptic systems are certainly ill-posed for initial value problems (Hadamard 1923; Renardy & Rogers 2004). However, we do not have a definite proof of well-posedness in the region of hyperbolicity because the relevant theory (*e.g.* Benzoni-Gavage & Serre 2007) has only been developed for hyperbolic systems that are either linear, or symmetrizable in the sense of Friedrichs (1954). Our systems are not symmetrizable, because the eigenvalues calculated below are not always real.

Following Whitham (1974), we write (2.3) and (2.2) as a quasilinear system of first-order partial differential equations,

$$\frac{\partial \boldsymbol{v}}{\partial t} + \mathbf{C}_x \cdot \frac{\partial \boldsymbol{v}}{\partial x} + \mathbf{C}_y \cdot \frac{\partial \boldsymbol{v}}{\partial y} + \boldsymbol{b} = 0, \tag{3.1}$$

where $\boldsymbol{v} = (u_1, v_1, h_1, \ldots, u_M, v_M, h_M)$ is the vector of dependent variables. Expressions for the matrix $\mathbf{C}_x$ and the vector $\boldsymbol{b}$ of algebraic terms are given in Appendix A for the case of two layers. Equation (3.1) is a system of $3M$ dependent variables and 3 independent variables. This system is formally hyperbolic (Whitham 1974, §5.9) if there are linear combinations of its $3M$ equations that transform the separate partial derivatives in t, x, y into directional derivatives of the components of $\boldsymbol{v}$ along directions that are confined to a two-dimensional characteristic surface $S(t, x, y) = 0$. Singularities in the solution propagate only along these surfaces, which generalise the characteristic curves for hyperbolic systems in one spatial dimension. The hyperbolicity property is thus independent of the algebraic terms in the vector $\boldsymbol{b}$, which includes all terms due to the traditional component of the Coriolis force.

Taking the inner product of (3.1) with a constant vector $\boldsymbol{\ell}$ yields

$$\sum_{m=1}^{3M} \left\{ \ell_m \frac{\partial v_m}{\partial t} + \left[\sum_{n=1}^{3M} \ell_n (C_x)_{n,m} \right] \frac{\partial v_m}{\partial x} + \left[\sum_{n=1}^{3M} \ell_n (C_y)_{n,m} \right] \frac{\partial v_m}{\partial y} \right\} + \sum_{m=1}^{3M} \ell_m b_m = 0. \tag{3.2}$$

The terms in braces $\{\cdots\}$ correspond to a directional derivative of v_m along the direction given by the coefficients of $(\partial_t v_m, \partial_x v_m, \partial_y v_m)$. Whitham's (1974) hyperbolicity condition for the system (3.1) requires the directions of the directional derivatives of $v_1, \ldots, v_{3M}$ to lie parallel to the surface $S(t, x, y) = 0$, and lie perpendicular to the normal $\nabla_t S$,

$$(\boldsymbol{\ell}, \boldsymbol{\ell} \cdot \mathbf{C}_x, \boldsymbol{\ell} \cdot \mathbf{C}_y) \cdot \nabla_t S = \boldsymbol{\ell} \cdot (\mathbf{I}, \mathbf{C}_x, \mathbf{C}_y) \cdot \nabla_t S = 0, \tag{3.3}$$

where $\nabla_t = (\partial_t, \partial_x, \partial_y)$ is the temporal/spatial gradient operator and and $\mathbf{I}$ is the $3M \times 3M$ identity matrix. This linear system of equations for $\boldsymbol{\ell}$ only has a non-zero solution when the determinant of the matrix $(\mathbf{I}, \mathbf{C}_x, \mathbf{C}_y) \cdot \nabla_t S$ is zero,

$$\left| \mathbf{I} \frac{\partial S}{\partial t} + \mathbf{C}_x \frac{\partial S}{\partial x} + \mathbf{C}_y \frac{\partial S}{\partial y} \right| = 0, \tag{3.4}$$

which defines the characteristic surfaces S close to a point (t_0, x_0, y_0) by relating the derivatives $\partial_t S$, $\partial_x S$, and $\partial_y S$ at that point.

Writing the normal at a point (t_0, x_0, y_0) as $(\partial_t S, \partial_x S, \partial_y S) = (-\omega, k_x, k_y)$ transforms (3.4) into

$$|k_x \mathbf{C}_x + k_y \mathbf{C}_y - \omega \mathbf{I}| = 0. \tag{3.5}$$

This relation between k_x, k_y, and ω defines the possible orientations of the surface $S = 0$ at (t_0, x_0, y_0), and hence the local shapes of the characteristic surfaces. Provided at least one of k_x and k_y are nonzero, we may write $k_x = k \cos\Theta$ and $k_y = k \sin\Theta$. Equation (3.5) then reduces to

$$|\cos\Theta \, \mathbf{C}_x + \sin\Theta \, \mathbf{C}_y - \lambda \mathbf{I}| = 0, \tag{3.6}$$

with $\lambda = \omega/k$ being the speed at which disturbances propagate in the direction Θ. The exceptional case with $k_x = k_y = 0$ has the characteristic surface tangent to the xy plane, so disturbances propagate with infinite speed. Equation (3.6) determines λ to be one of the eigenvalues $\lambda_1, \ldots, \lambda_{3M}$ of the matrix $\cos\Theta\,\mathbf{C}_x + \sin\Theta\,\mathbf{C}_y$, and (3.3) shows that $\boldsymbol{\ell}_1, \ldots, \boldsymbol{\ell}_{3M}$ are the corresponding left eigenvectors. These eigenvalues determine the speeds at which disturbances propagate, or equivalently the gradients of the corresponding characteristic surfaces S_j with respect to the t-axis. The system (3.1) is not hyperbolic if, for any value of Θ, one or more of the eigenvalues λ_j becomes complex. The corresponding characteristic surface S_j is then at least partly complex.

In summary, for given values of the dependent variables $\boldsymbol{v}$ in $\mathbf{C}_x$ and $\mathbf{C}_y$, the system (3.1) is hyperbolic if, for all real Θ, the matrices $\cos\Theta\,\mathbf{C}_x + \sin\Theta\,\mathbf{C}_y$ possess only real eigenvalues, and complete sets of eigenvectors. This is taken as the fundamental condition for hyperbolicity in more recent work such as Godlewski & Raviart (1996) and Benzoni-Gavage & Serre (2007), instead of Whitham's (1974) condition based on characteristic surfaces. Establishing the hyperbolicity of a system in two spatial dimensions is thus equivalent to establishing the hyperbolicity of the reduced one-dimensional system for disturbances propagating at an arbitrary angle Θ with respect to the xy axes. As our system (2.3)–(2.2) is expressed in a vector-invariant form, we may absorb the angle Θ by a suitable rotation of the axes before expressing (2.3)–(2.2) in components. Establishing the hyperbolicity of the system (2.3)–(2.2) thus reduces to verifying that the eigenvalues of $\mathbf{C}_x$ are real for all angles of propagation θ as defined in (2.1).

4. Hyperbolicity of the two-layer shallow water equations

We first focus on the two-layer shallow water equations ($M = 2$), because they are the simplest case of (2.3)–(2.2) that allow velocity and density jumps between adjacent layers. Being analytically tractable, they provide a useful illustration of the behaviour found in cases with three or more layers. Following the hyperbolicity criterion of §3, the two-layer shallow water equations are hyperbolic for given values of u_1, v_2, h_1, u_2, v_2 and h_2 if all eigenvalues of the matrix $\mathbf{C}_x$, given in Appendix A, are real. The layer densities appear only via the relative density difference $\sigma = 1 - \rho_1/\rho_2$, which must satisfy $0 < \sigma < 1$ for the fluid to be stably stratified. Two of the eigenvalues of $\mathbf{C}_x$ are simply $\lambda_5 = u_1$ and $\lambda_6 = u_2$. The remaining four eigenvalues $\lambda_1, \ldots, \lambda_4$ are the roots of the quartic polynomial given in Appendix B.

4.1. *Traditional two-layer equations*

Relatively simple formulae are available for the special case of equal equilibrium layer thicknesses ($h_1 = h_2 = 1/2$) under the traditional approximation ($\varepsilon = 0$) so that the hyperbolicity is unaffected by rotation. The quartic (B 1) then has roots (Houghton & Isaacson 1970; Liska & Wendroff 1997)

$$\lambda = \frac{1}{2}\,(u_1 + u_2) \pm_\alpha \frac{1}{2}\sqrt{2 + (u_2 - u_1)^2 \pm_\beta 2\sqrt{1 - \sigma + 2\,(u_2 - u_1)^2}}, \tag{4.1}$$

where $\pm_\alpha$ and $\pm_\beta$ may take signs independently. These roots give the wave speeds for the non-rotating two-layer shallow water equations, linearised around constant velocities $\boldsymbol{u}_1, \boldsymbol{u}_2$ and heights $h_1 = h_2 = 1/2$.

Two of these wave speeds become complex when the difference between the velocities parallel to the x-axis lies in the range

$$\left[\frac{1}{2}\left(1 - \sqrt{1-\sigma}\right)\right]^{1/2} < \frac{1}{2}|u_2 - u_1| < \left[\frac{1}{2}\left(1 + \sqrt{1-\sigma}\right)\right]^{1/2}. \tag{4.2}$$

The lower and upper limits are the internal and surface gravity wave speeds respectively, so the eigenvalues are always real when half the velocity difference $\frac{1}{2}|u_2 - u_1|$ is smaller than the internal gravity wave speed, or larger than the surface gravity wave speed. This offers a physical interpretation for (4.2): the interface between the layers becomes subject to Kelvin–Helmholtz instablities when the velocity difference exceeds twice the internal gravity wave speed, so linear perturbations grow with time. However, when the velocity difference exceeds twice the surface gravity wave speed, disturbances in the two layers are advected away from each other before they can grow. By the analysis in §3, the two-layer shallow water equations are ill-posed if the absolute velocity difference between the layers lies within the range (4.2).

4.2. *The nature of the roots of a quartic*

There are exact formulae for the roots of a general quartic (*e.g.* Abramowitz & Stegun 1965), but these expressions become prohibitively complicated for non-equal layer thicknesses ($h_1 \neq h_2$), or under the complete Coriolis force ($\varepsilon \neq 0$). Instead, following the approach used by Lawrence (1990) for the non-rotating two-layer equations, the nature of the roots may be determined from the discriminant of the quartic and other related quantities (Wang & Qi 2005).

The discriminant $\mathcal{D}$ of a quartic with roots $\lambda_1, \lambda_2, \lambda_3, \lambda_4$ is (*e.g.* Irving 2004)

$$\mathcal{D} = (\lambda_1 - \lambda_2)^2\,(\lambda_1 - \lambda_3)^2\,(\lambda_1 - \lambda_4)^2\,(\lambda_2 - \lambda_3)^2\,(\lambda_2 - \lambda_4)^2\,(\lambda_3 - \lambda_4)^2, \tag{4.3}$$

defined up to an arbitrary multiplicative constant. The coefficients in the quartic (B 1) are all real, so the roots are either

real, or occuring in complex conjugate pairs. The quartic has two real roots and two complex conjugate roots when the discriminant $\mathcal{D} < 0$. When $\mathcal{D} \geqslant 0$ the quartic has either four real roots or two pairs of complex conjugate roots.

The discriminant $\mathcal{D}$, and the nature of the roots when $\mathcal{D} \geqslant 0$, may be determined from the coefficients of a quartic polynomial without finding the roots explicitly (Garver 1933; Ku 1965; Wang & Qi 2005). Following Ku (1965), we consider a quartic of the form

$$a_0\lambda^4 + 4a_1\lambda^3 + 6a_2\lambda^2 + 4a_3\lambda + a_4 = 0, \tag{4.4}$$

with real coefficients $a_0, \ldots, a_4$ with $a_0 > 0$, and define the quantities

$$\mathcal{G} = a_0^2a_3 - 3a_0a_1a_2 + 2a_1^3, \qquad \mathcal{H} = a_0a_2 - a_1^2, \qquad \mathcal{I} = a_0a_4 - 4a_1a_3 + 3a_2^2,$$
$$\mathcal{J} = \begin{vmatrix} a_0 & a_1 & a_2 \\ a_1 & a_2 & a_3 \\ a_2 & a_3 & a_4 \end{vmatrix}, \qquad \mathcal{K} = 12\mathcal{H}^2 - a_0^2\mathcal{I}, \qquad \mathcal{D} = \mathcal{I}^3 - 27\mathcal{J}^2. \tag{4.5}$$

This expression for $\mathcal{D}$ is equivalent to our previous definition (4.3). Wang & Qi (2005) proved that the quartic (4.4) has no real roots if and only if

$$\text{(i) } \mathcal{D} = 0,\ \mathcal{G} = 0,\ \mathcal{K} = 0, \text{ and } \mathcal{H} > 0; \text{ or} \tag{4.6a}$$
$$\text{(ii) } \mathcal{D} > 0; \text{ and (a) } \mathcal{H} \geqslant 0; \text{ or (b) } \mathcal{H} < 0 \text{ and } \mathcal{K} < 0. \tag{4.6b}$$

Otherwise, all four roots are real when $\mathcal{D} \geqslant 0$.

For example, the case of equal layer thicknesses ($h_1 = h_2 = 1/2$) under the traditional approximation ($\varepsilon = 0$) in the quartic (B 1) gives the discriminant

$$\mathcal{D} = \left((u_2 - u_1)^4 - 4\,(u_2 - u_1)^2 + 4\,\sigma\right)\left(1 - \sigma + 2\,(u_2 - u_1)^2\right)^2. \tag{4.7}$$

Solving the first bracket for $|u_2 - u_1|$ and comparing with (4.1) shows that all four roots are real when $\mathcal{D} \geqslant 0$, and two roots are complex when $\mathcal{D} < 0$. However, the discriminant alone does not distinguish between the cases of four real roots and four complex roots. Evaluating

$$\mathcal{H} = -\frac{1}{12}\left(2 + (u_2 - u_1)^2\right) < 0, \qquad \mathcal{K} = \frac{1}{4}\left(1 - \sigma + 2(u_2 - u_1)^2\right) > 0. \tag{4.8}$$

and comparing with (4.6*a*,b) shows all four roots of (B 1) with $h_1 = h_2$ and $\varepsilon = 0$ are real when $\mathcal{D} \geqslant 0$, so the shallow water equations are hyperbolic. For $\mathcal{D} < 0$, two roots are complex and the shallow water equations are ill-posed.

Even when $h_1 \neq h_2$, it is still possible to obtain exact expressions for the quantities $\mathcal{H}$ and $\mathcal{K}$ when $\varepsilon = 0$,

$$\mathcal{H} = -\frac{1}{12}\left[2(h_1 + h_2) + (u_2 - u_1)^2\right] < 0, \tag{4.9a}$$

$$\mathcal{K} = \frac{1}{4}\left[(h_1 - h_2)^2 + 4h_1h_2(1 - \sigma) + 2(h_1 + h_2)(u_2 - u_1)^2\right] > 0. \tag{4.9b}$$

These reduce to the formulae in (4.8) when $h_1 = h_2 = 1/2$. The traditional shallow water equations with unequal layer depths ($h_1 \neq h_2$) are thus hyperbolic for $\mathcal{D} \geqslant 0$ and non-hyperbolic for $\mathcal{D} < 0$. The discriminant $\mathcal{D}$ depends only on the velocity difference $U = |u_2 - u_1|$, the density ratio σ, and the layer thicknesses h_1 and h_2.

4.3. *Asymptotic expansion in σ*

The method outlined in §4.2 makes determining the nature of the roots of (B 1) much simpler, but even the quantities defined in (4.6*a*,b) become intractably complicated when $h_1 \neq h_2$ and $\varepsilon \neq 0$. However, the relative density difference σ between adjacent layers is very small in any oceanographic context. An asymptotic expansion in σ gives a tractable sufficient condition for hyperbolicity that closely approximates the traditional ($\varepsilon = 0$) hyperbolicity condition at leading order.

The discriminants calculated in §4.2 depend only on the velocity difference $U = |u_2 - u_1|$, the relative density difference σ, and the layer thicknesses h_1 and h_2. We therefore seek the critical velocity difference $U = U_c(h_1, h_2; \sigma)$ at which $\mathcal{D} = 0$. In the case of equal layer depths, the smaller critical velocity difference in (4.2) scales as $U_c \sim \sigma^{1/2}$ as $\sigma \to 0$, so we pose asymptotic expansions of U_c and $\mathcal{D}$ in powers of $\sigma^{1/2}$,

$$U_c = U_c^{(0)} + \sigma^{1/2}U_c^{(1)} + \sigma U_c^{(2)} + \cdots, \qquad \mathcal{D} = \mathcal{D}^{(0)} + \sigma^{1/2}\mathcal{D}^{(1)} + \sigma\mathcal{D}^{(2)} + \cdots. \tag{4.10}$$

We obtain the $U_c^{(0)}, U_c^{(1)}, \ldots$ by successively solving $\mathcal{D}^{(0)} = 0$, $\mathcal{D}^{(1)} = 0$, $\mathcal{D}^{(2)} = 0$, etc. The first terms in the expansion

yield the approximate conditions

$$U > U_{c1} = \sigma^{1/2}\sqrt{h_1 + h_2} + O(\sigma^{3/2}), \quad \text{and} \tag{4.11a}$$

$$U < U_{c2} = \left(h_1^{1/3} + h_2^{1/3}\right)^{3/2} + O(\sigma), \tag{4.11b}$$

under which the two-layer shallow water equations are ill-posed. These coincide with the leading order terms in an expansion of (4.2) in σ when $h_1 = h_2 = 1/2$. Liska & Wendroff (1997) previously obtained the upper limit (4.11*b*) for the case $\sigma = 0$, and Long (1956) obtained the lower limit (4.11*a*) for the two-layer shallow water equations with a rigid lid. The lower limit U_{c1} coincides with the leading order in σ approximation to the internal wave speed.

4.4. *Rescaling by the internal gravity wave speed*

For the non-traditional two-layer shallow water equations ($\varepsilon \neq 0$), even the zeros of the leading-order discriminant $\mathcal{D}^{(0)}$ are too complicated to solve directly, as they no longer depend solely on $|u_2 - u_1|$, the difference in the velocity components parallel to the x-axis. We now demonstrate that rescaling the two-layer equations by the internal gravity wave speed instead of the surface wave speed leads naturally to the asymptotic expansion in σ presented in the previous subsection. This allows us to calculate the lower bound in (4.2), but excludes the upper bound as being asymptotically large. This rescaling is equivalent to adopting the Boussinesq version of the multi-layer shallow water equations, as studied by Chumakova *et al.* (2009*a*,*b*) in the absence of rotation.

Under the traditional approximation, the two-layer equations remain hyperbolic as long as $U < U_{c1}$, where U_{c1} defined in (4.11*a*) is proportional to $\sigma^{1/2}$, the dimensionless internal gravity wave speed. This suggests that a rescaling based on the internal gravity wave speed, internal deformation radius, and corresponding internal non-traditional parameter,

$$c' = \sqrt{\sigma g H}, \qquad R'_{\mathrm{d}} = \frac{c'}{2\tilde{\Omega}}, \qquad \varepsilon' = 2\tilde{\Omega}\sqrt{\frac{H}{\sigma g}}, \tag{4.12}$$

will capture the loss of hyperbolicity when $U \sim \sigma^{1/2} \ll 1$. Non-dimensionalising (2.3)–(2.2) using these scales is equivalent to setting

$$\boldsymbol{u}_1 = \sigma^{1/2}u'_1, \qquad \boldsymbol{u}_2 = \sigma^{1/2}u'_2, \qquad \lambda = \sigma^{1/2}\lambda', \qquad \varepsilon = \sigma^{1/2}\varepsilon', \tag{4.13}$$

in the quartic polynomial (B 1) for the eigenvalues of $\mathbf{C}_x$. The rescaled variables, denoted by primes ($'$), are assumed to remain $O(1)$ as $\sigma \to 0$. We write the rescaled quartic in a form that matches (4.4),

$$\sigma\lambda'^4 + \sigma\left(\varepsilon'\Omega_y(h_1 + h_2) - 2(u'_1 + u'_2)\right)\lambda'^3 + 6a_2\lambda'^2 + 4a_3\lambda' + a_4 = 0, \tag{4.14}$$

where the expressions for the coefficients a_2, a_3 and a_4 are similar to those in (B 1). Under the traditional approximation ($\varepsilon' = 0$) and with equal layer depths ($h_1 = h_2 = 1/2$) two of the eigenvalues λ' are complex for the same range of velocity differences as (4.2),

$$\left[\frac{1}{2\sigma}\left(1 - \sqrt{1-\sigma}\right)\right]^{1/2} < \frac{1}{2}|u'_1 - u'_2| < \left[\frac{1}{2\sigma}\left(1 + \sqrt{1-\sigma}\right)\right]^{1/2}. \tag{4.15}$$

Under this scaling the upper limit in (4.15), which is equal to the dimensionless surface gravity wave speed, approaches infinity as $\sigma \to 0$. An asymptotic expansion in σ thus excludes this upper limit, and captures only the lower limit.

4.5. *Properties of the roots*

We now pose asymptotic expansions in σ of the quantities $\mathcal{D}$, $\mathcal{H}$, $\mathcal{K}$ for the rescaled quartic (4.14) under the complete Coriolis force ($\varepsilon \neq 0$). We seek only the leading-order solution, so we omit the superscript $^{(n)}$ notation for terms in our expansions. This corresponds to making the Boussinesq approximation, and allows us to characterise the hyperbolicity of the two-layer equations over the entire parameter space.

Expanding the quantities $\mathcal{H}$ and $\mathcal{K}$ from (4.5) in powers of σ yields

$$\mathcal{H} = -\frac{1}{6}\sigma(h_1 + h_2) + O(\sigma^2), \qquad \mathcal{K} = \frac{1}{4}\sigma^2(h_1 + h_2)^2 + O(\sigma^3), \tag{4.16}$$

so $\mathcal{H} < 0$ and $\mathcal{K} > 0$ for sufficiently small σ. Using conditions (4.6*a*,b), $\mathcal{D} \geqslant 0$ implies four real eigenvalues, and $\mathcal{D} < 0$ implies two real and two complex eigenvalues. Expanding $\mathcal{D}$ in powers of σ yields

$$\mathcal{D} = -\frac{1}{16}\sigma h_1 h_2(h_1 + h_2)\left[(u'_2 - u'_1)^2 - \varepsilon'\Omega_x(h_1 + h_2)(v'_2 - v'_1) - (h_1 + h_2)\left(1 + \frac{1}{4}\varepsilon'^2\Omega_x^2(h_1 + h_2)^2\right)\right] + O(\sigma^2). \tag{4.17}$$

The prefactor $-(1/16)\sigma h_1 h_2 (h_1 + h_2)$ in (4.17) is strictly negative, so for sufficiently small σ, the nature of the roots is determined by the sign of the expression in square brackets. The form of this expression allows us to simplify our notation, as it depends on the velocity component differences $u_2' - u_1'$ and $v_2' - v_1'$, but not on the absolute velocities in either layer. We therefore write the velocity difference as

$$u_2' - u_1' = U' \cos\psi, \qquad v_2' - v_1' = U' \sin\psi, \tag{4.18}$$

in terms of its magnitude $U' \geqslant 0$ and an angle $\psi \in [0, 2\pi)$. The angles $\psi = 0, \pi$ correspond to a velocity difference in the x-direction, and the angles $\psi = \pm\pi/2$ correspond to a velocity difference in the y-direction. We may choose $h_1 + h_2 = 1$ without loss of generality, since the vertical length scale H is arbitrary in our nondimensionalisation (2.4). Finally, ε', θ and ϕ appear only in the combination $\varepsilon' \sin\theta \cos\phi$, so we introduce the dimensionless quantities

$$\tilde{\varepsilon} = (1/2)\, \varepsilon' \cos\phi, \qquad \hat{\varepsilon} = \tilde{\varepsilon} \sin\theta = \tilde{\Omega}_x H / c', \tag{4.19}$$

where $\tilde{\Omega}_x$ is the dimensional x-component of the rotation vector. The quantity $\hat{\varepsilon}$ measures the ratio of the internal wave speed c' to the velocity parallel to the y-axis acquired by a fluid parcel that is raised through a vertical distance H while conserving angular momentum. This ratio may be positive or negative, depending on the orientation θ of the axes. The component $\tilde{\Omega}_y$ of the rotation vector does not appear in the leading-order discriminant.

As in §4.3, we seek the leading-order critical velocity difference $U' = U_c'(\psi, \hat{\varepsilon})$ at which the two-layer equations lose hyperbolicity. Substituting (4.18) and (4.19) into (4.17) yields

$$U_c'^2 \cos^2\psi - 2\hat{\varepsilon} U_c' \sin\psi - (1 + \hat{\varepsilon}^2) = 0. \tag{4.20}$$

Under the traditional approximation ($\hat{\varepsilon} = 0$), this reduces to

$$U_c' \, |\cos\psi| = 1. \tag{4.21}$$

The traditional two-layer equations are thus hyperbolic for

$$|u_2' - u_1'| < 1 + O(\sigma), \text{ or } |u_2 - u_1| < \sigma^{1/2} + O(\sigma^{3/2}), \tag{4.22}$$

which matches the lower limit U_{c1} from (4.11a) with $h_1 + h_2 = 1$, as obtained via an asymptotic expansion in σ under the external scaling (2.4). For $\hat{\varepsilon} \neq 0$, the left hand side of equation (4.20) is a quadratic polynomial in U_c' with one strictly negative root, which we discard because we imposed $U_c' \geqslant 0$ when specifying our polar coordinates in (4.18), and one strictly positive root,

$$U_c' = \frac{1}{\cos^2\psi} \left(\hat{\varepsilon} \sin\psi + \sqrt{\cos^2\psi + \hat{\varepsilon}^2} \right). \tag{4.23}$$

The non-traditional equations with $\hat{\varepsilon} \neq 0$ may thus become ill-posed due to a non-zero transverse shear $|v_2' - v_1'|$, even for vanishing parallel shear, $|u_2' - u_1'| = 0$. Substituting $u_2' - u_1' = 0$ into (4.17) shows that the equations lose hyperbolicity ($\mathcal{D} < 0$) when

$$v_1' - v_2' > \frac{1 + \hat{\varepsilon}^2}{2\hat{\varepsilon}}. \tag{4.24}$$

In §6 we show that this loss of hyperbolicity in our two-layer shallow water equations corresponds to an instability to transverse shear in a continuously stratified fluid.

In figure 2 we plot the curve $\mathcal{D} = 0$ in velocity space for typical parameters and a stationary upper layer ($u_1' = v_1' = 0$). We have calculated this curve using both our traditional (4.21) and non-traditional (4.23) leading-order asymptotic solutions, and also numerically using a bisection search to find the velocity difference U_c' at which the unapproximated discriminant $\mathcal{D}$ vanishes for each ψ. The asymptotic and numerical solutions show such good agreement that we have had to use a very large density difference ($\sigma = 0.3$) in figure 2(a) to illustrate the difference between them. The curves are indistinguishable for the more realistic value of $\sigma = 10^{-3}$ in figure 2(b).

4.6. *Loss of hyperbolicity due to shear under the complete Coriolis force*

We showed in §3 that the multilayer shallow water equations are hyperbolic if infinitesimally short disturbances propagate stably in every direction Θ. This is equivalent to requiring that the matrix $\mathbf{C}_x$ have real eigenvalues for all orientations θ of the x and y axes, subject to the orientation of the velocity vector remaining fixed relative to the geographical East/North axes. We therefore define the angle $\Psi = \theta + \psi$ between the velocity vector and the East axis, and determine the maximum velocity difference U_m' for fixed Ψ. The two-layer equations are hyperbolic for $U' < U_m'(\Psi)$, where

$$U_m'(\Psi) = \min_{\theta \in [0, 2\pi)} \left\{ U_c' \left(\Psi - \theta, \hat{\varepsilon}(\theta) \right) \right\}. \tag{4.25}$$

For example, under the traditional approximation ($\varepsilon' = 0$), the maximum velocity difference $U_m'(\Psi)$ is

$$U_m'(\Psi) = \min_{\theta \in [0, 2\pi)} \left\{ U_c' \left(\Psi - \theta, 0 \right) \right\} = \min_{\theta \in [0, 2\pi)} |\sec(\Psi - \theta)| = 1. \tag{4.26}$$

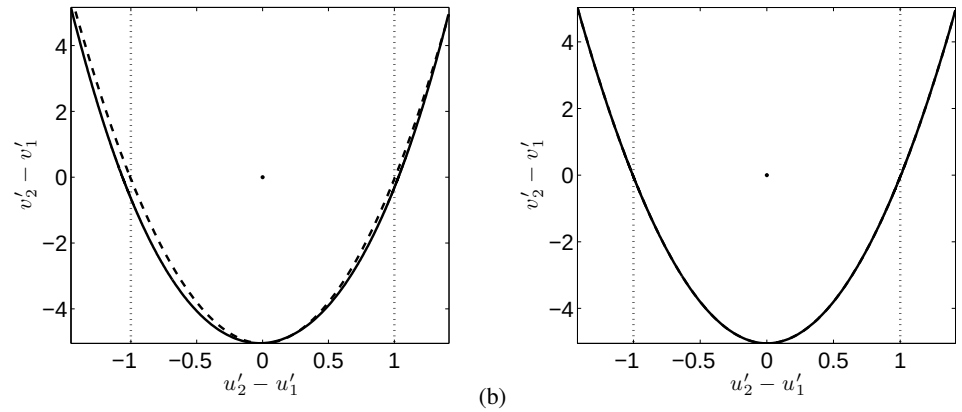

FIGURE 2. Plots of the curve $\mathcal{D} = 0$ for $\boldsymbol{u}_1 = \boldsymbol{0}$, $h_1 = h_2 = 1/2$, $\phi = \pi/4$, $\theta = \pi/4$, and $\varepsilon = 0.4$, with (a) $\sigma = 0.3$ and (b) $\sigma = 10^{-3}$. The curves have been obtained using our asymptotic solution in §4.5 under the traditional approximation (dotted lines) and under the complete Coriolis force (dashed lines), and also via a numerical bisection search of the unapproximated discriminant (4.5).

Thus, to leading order in σ, the two-layer equations lose hyperbolicity if the magnitude of the velocity difference exceeds the internal wave speed.

Under the complete Coriolis force ($\varepsilon' \neq 0$) it is less straightforward to calculate U_m', as U_c' depends on θ via both $\psi = \Psi - \theta$ and $\hat{\varepsilon} = (1/2)\varepsilon' \cos\phi \sin\theta$. We proceed by first calculating the minimum of $U_c'(\psi, \hat{\varepsilon})$ over all ψ for fixed $\hat{\varepsilon}$. The stationary points are

$$\frac{\partial U_c'}{\partial \psi} = 0 \quad \text{and} \quad \begin{cases} U_c' = 1, & \text{at } \psi = \sin^{-1}(-\hat{\varepsilon}), \quad \text{for } |\hat{\varepsilon}| \leqslant 1, \\ U_c' = (\hat{\varepsilon} + 1/\hat{\varepsilon})/2, & \text{at } \psi = \pi\,(1 + \operatorname{sgn}(\hat{\varepsilon})/2), \quad \text{for } |\hat{\varepsilon}| \geqslant 1. \end{cases} \tag{4.27}$$

Therefore, for any θ such that $|\hat{\varepsilon}| < 1$, there exist two values of $\psi \in [0, 2\pi)$ for which $U_c'(\psi, \hat{\varepsilon})$ takes its minimum value of 1. For any θ such that $|\hat{\varepsilon}| \geqslant 1$, the critical velocity difference satisfies $U_c' \geqslant 1$ for all $\psi \in [0, 2\pi]$. Thus $U_m'(\Psi)$ has 1 as a lower bound, but this does not guarantee that $U_m'(\Psi) = 1$ for all Ψ. We therefore fix $\Psi = \theta + \psi$ so that condition (4.27) may be interpreted as a statement that $U_c' = 1$ at

$$\sin(\Psi - \theta) + \tilde{\varepsilon} \sin\theta = 0, \text{ or at } \tan\theta = \frac{\sin\Psi}{\cos\Psi - \tilde{\varepsilon}}. \tag{4.28}$$

For any $\Psi \in [0, 2\pi)$, there exists $\theta \in [0, 2\pi)$ such that $U_c'(\Psi - \theta, \tilde{\varepsilon}\sin\theta) = 1$, so $U_m'(\Psi) = 1$ for all Ψ. Thus, to leading order in σ, the traditional and non-traditional shallow water equations are both hyperbolic when the magnitude of the velocity differences is smaller than the internal wave speed. However, the shape of the domain of hyperbolicity changes substantially due to non-traditional effects, as shown in figure 2, and again in figure 3 below.

4.7. *Loss of hyperbolicity due to the Eötvös effect*

The results presented in the preceding section are only valid when the eastward velocities in the layers are not too large. When the eastward velocity in either layer is sufficiently large, the upward acceleration due to the non-traditional component of the Coriolis force may counteract the downward acceleration due to gravity. This is known as the Eötvös effect (*e.g.* Persson 2005). Though such large velocities will not arise in the context of geophysical fluid dynamics, we include a brief discussion here to complete our analysis.

For simplicity, we restrict our attention to a large eastward velocity in the lower layer, setting $\boldsymbol{u}_1 = 0$ and defining the northward and eastward velocities in the lower layer as $u_\mathrm{n} = u_2 \sin\theta + v_2 \cos\theta$ and $u_\mathrm{e} = u_2 \cos\theta - v_2 \sin\theta$ respectively. It is convenient to take only u_e or u_n nonzero at first. Setting $u_\mathrm{n} = 0$, we may rewrite the unapproximated discriminant $\mathcal{D}$ of (B 1) as a polynomial in u_e,

$$\begin{aligned} \mathcal{D} = &- 4h_1h_2\varepsilon \cos\phi \cos^8\theta \left(4 + \varepsilon^2 h_1 \cos^2\phi\right) u_\mathrm{e}^9 \\ &+ h_1h_2 \cos^6\theta \left(4 + \varepsilon^2 h_1 \cos^2\phi\right) \Big[4\cos^2\theta \\ &\quad + \varepsilon^2 \cos^2\phi \left(-4h_1 \cos^2\theta(3 + \sigma) + h_2\left(1 - 17\sin^2\theta\right)\right)\Big] u_\mathrm{e}^8 + O\left(u_\mathrm{e}^7\right). \end{aligned} \tag{4.29}$$

The coefficient of u_e^9 is strictly negative, so when $\varepsilon > 0$ the discriminant $\mathcal{D}$ is negative for sufficiently large and positive u_e. Only when $\varepsilon = 0$ is the discriminant positive for arbitrarily large u_e. For $\cos\theta \neq 0$, the form of (4.29) motivates an asymptotic expansion of the critical value of u_e of the form $u_\mathrm{e} = \varepsilon^{-1} u_\mathrm{e}^{(-1)} + u_\mathrm{e}^{(0)} + \varepsilon u_\mathrm{e}^{(1)} + \cdots$. Substituting this expansion

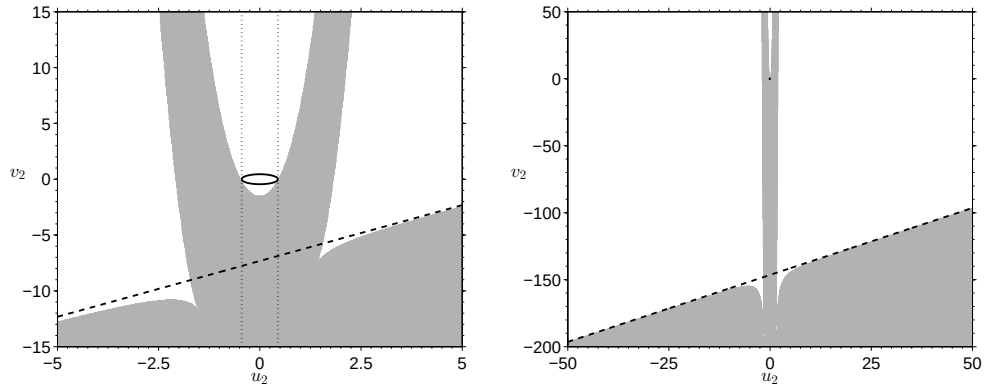

(a) (b)

FIGURE 3. The shaded regions indicate which values of the lower-layer velocity $\boldsymbol{u}_2$ give complex eigenvalues of the Jacobian matrix $\mathbf{C}_x$. The upper layer velocity is zero, $\phi = \pi/12$, $\theta = \pi/4$, and $h_1 = h_2 = 1/2$. Panel (a) shows the region $\sigma = \varepsilon = 0.2$, and panel (b) shows the region for $\sigma = \varepsilon = 0.01$. Also plotted are the circles $|\boldsymbol{u}_2| = \sqrt{\sigma}$, the diagonal lines $u_e = \varepsilon^{-1} \sec\phi$ marking loss of hyperbolicity due to the Eötvös effect, and two vertical lines marking the region $|u_2| < \sqrt{\sigma}$ inside which the traditional two-layer shallow water equations are hyperbolic. The circle appears as an ellipse in panel (a) due to the different scales on the two axes, and as a dot in panel (b). The circles are tangent to the boundaries of the ill-posed regions shown in grey, in accordance with the analysis at the end of §4.5.

into (4.29) and solving $\mathcal{D} = 0$, we find $u_{\mathrm{e}}^{(-1)} = 1/\cos\phi$ and $u_{\mathrm{e}}^{(0)} = 0$. Thus $\mathcal{D} < 0$ when

$$u_{\mathrm{e}} > \frac{1}{\varepsilon\,\cos\phi} + O(\varepsilon). \tag{4.30}$$

This condition is independent of the direction of wave propagation θ, so (4.30) is sufficient for the system to be ill-posed. This matches the condition found by Dellar & Salmon (2005) for the hyperbolicity of the single-layer shallow water equations with complete Coriolis force. We may derive an analogous result for large eastward velocities in the upper layer. We also find $\mathcal{D} > 0$ for sufficiently large eastward velocities in both layers, because all four roots of (B 1) become complex.

To study the effect of large northward/southward velocities, we set $u_{\mathrm{e}} = 0$ and write $\mathcal{D}$, $\mathcal{H}$, $\mathcal{K}$ as polynomials in u_{n},

$$\mathcal{D} = h_1 h_2 \sin^8\theta \left(4 + \varepsilon^2 h_1 \cos^2\phi\right)\left(4 + \varepsilon^2\cos^2\phi\,(4h_1(1-\sigma) + h_2)\right) u_{\mathrm{n}}^8 + O\left(u_{\mathrm{n}}^7\right), \tag{4.31a}$$

$$\mathcal{H} = -\tfrac{1}{3}\sin^2\theta u_{\mathrm{n}}^2 + O\left(u_{\mathrm{n}}\right), \tag{4.31b}$$

$$\mathcal{K} = 8\sin^2\theta\left(h_1 + h_2 + \varepsilon^2\cos^2\phi\left(h_1h_2(1-\sigma) + \tfrac{1}{4}(h_1^2 + h_2^2)\right)\right) u_{\mathrm{n}}^2 + O\left(u_{\mathrm{n}}\right). \tag{4.31c}$$

For $\sin\theta \neq 0$, these quantities satisfy $\mathcal{D} > 0$, $\mathcal{H} < 0$, $\mathcal{K} > 0$ as $u_{\mathrm{n}} \to \pm\infty$, so all roots of (B 1) are real by (4.6*b*). The same result holds for large northward/southward velocities in the upper layer.

We illustrate our results from this and the previous section in figure 3. We have computed the region of lower-layer velocities $\boldsymbol{u}_2$ for which some eigenvalues of the Jacobian matrix $\mathbf{C}_x$ are complex. In this calculation the upper layer is stationary, and we have used specimen parameters $\phi = \pi/12$, $\theta = \pi/4$, $h_1 = h_2 = 1/2$. Figure 3(a) uses exaggerated values of σ and ε to illustrate the qualitative features of the region close to $\boldsymbol{u}_2 = 0$. The eigenvalues become complex when $|u_2|$ becomes too large, but then become real again for even larger $|u_2|$, as they do under the traditional approximation. However, with the complete Coriolis force they also become complex when v_2 becomes too large and negative, or when the eastward velocity is very large. The same qualitative features are present in figure 3(b) with more realistic values of σ and ε. The latter case shows a very clear separation between the two asymptotic regimes examined above – the regime of very small velocity difference between the layers, and the regime of very large absolute velocities within the layers. The boundaries of these two regimes are shown by an ellipse (due to the unequal axis scales) and a dashed line respectively. The ellipses are tangent to the boundaries of the ill-posed regions shown in grey, in accordance with the analysis at the end of §4.5.

5. Hyperbolicity of the multilayer shallow water equations

In §4 we restricted our attention to the two-layer shallow water equations because they are the most analytically tractable, and thus serve as a useful illustration of the situations in which (2.3)–(2.2) lose hyperbolicity. For the purposes of predictive numerical ocean models that use a shallow water-like formulation (*e.g.* Bleck *et al.* 1992; Bleck & Chassignet 1994; Adcroft & Hallberg 2006), it is more pertinent to determine the hyperbolicity for arbitrarily many layers. The $3M \times 3M$ matrix analogous to $\mathbf{C}_x$ has $3M$ eigenvalues, M of which are the components parallel to the wavevector of the fluid velocities in the M layers. The remaining eigenvalues are determined by the roots of a $2M$-degree polynomial in λ, so obtaining analytical constraints on the eigenvalues quickly becomes intractable for $M \geqslant 3$. In this section we restrict our attention to the three-

layer equations because they illustrate the generalisation of our two-layer results to multiple layers, yet their domain of hyperbolicity may still be characterised by a relatively small number of parameters.

The eigenvalues of $\mathbf{C}_x$ for $M = 3$ are determined by a sixth-order polynomial in λ, analogous to (B 1). As in §4.5 we focus on the Boussinesq limit $\sigma \to 0$ that is most relevant to geophysical flows, and only permits loss of hyperbolicity due to shear. Following the approach described in §4.4, we rescale the three-layer shallow water equations (2.3)–(2.2) using the internal gravity wave speed and internal deformation radius. The rescaled characteristic polynomial has the form

$$\sigma\lambda'^6 + \sigma\left(\varepsilon\Omega_y(h_1+h_2+h_3) - 2(u_1'+u_2'+u_3')\right)\lambda'^5 + a_2\lambda'^4 + a_3\lambda'^3 + a_4\lambda'^2 + a_5\lambda' + a_6 = 0, \quad (5.1)$$

analogous to (4.14). For simplicity we assume equal relative density contrasts between the layers, $\sigma = (\rho_2 - \rho_1)/\rho_2 = (\rho_3 - \rho_2)/\rho_3$, but permit variations of the layer thicknesses h_1, h_2 and h_3. This is conceptually similar to altering the density contrasts, in that it modifies the stratification represented by the three constant densities in the three layers.

In §4.5 we posed an asymptotic expansion of the discriminant of (4.14) in powers of σ to determine the nature of its roots. Figure 2 showed that the resulting domain of hyperbolicity is indistinguishable from that of the unapproximated two-layer shallow water equations, even when σ is much larger than any plausible oceanic value. The domain of hyperbolicity at leading order in σ may equivalently be obtained by posing an asymptotic expansion of the quartic (4.14) in powers of σ, and determining the roots of the leading-order polynomial. For example, setting $\sigma = 0$ in (4.14) yields a quadratic polynomial in λ', whose discriminant is identical to (4.17). Similarly, rather than considering the discriminant for the full sixth-order polynomial (5.1), we pose an asymptotic expansion of (5.1) in σ and retain only the $O(1)$ terms. This approach precludes the calculation of $O(\sigma)$ and higher corrections to the hyperbolicity condition. Setting $\sigma = 0$ in (5.1) yields the quartic equation

$$(h_1+h_2+h_3)\,\lambda'^4 + +a_3^{(0)}\lambda'^3 + a_4^{(0)}\lambda'^2 + a_5^{(0)}\lambda' + a_6^{(0)} = 0, \quad (5.2)$$

where $a_i^{(0)} = a_i|_{\sigma=0}$ is the leading-order i^{th} coefficient of (5.1). As in §4.5, the coefficients in (5.2) only depend on ε', θ and ϕ via the modified aspect ratio $\hat{\varepsilon}$ defined in (4.19).

We determine the nature of the roots of (5.2) using the method outlined in §4.2. All of the quantities in (4.5) depend only on the velocity differences between layers, rather than on the absolute velocities. For example, in the special case of equal layer depths ($h_1 = h_2 = h_3 = 1/3$) we find

$$\mathcal{H} = -1 + \hat{\varepsilon}\,(v_1 - v_3) - (5/6)\hat{\varepsilon}^2. \quad (5.3)$$

From (4.6*b*), we expect that (5.2) may have four complex eigenvalues when $\mathcal{H} \geqslant 0$, or when

$$v_1' - v_3' \geqslant \hat{\varepsilon}^{-1} + (5/6)\hat{\varepsilon}, \quad (5.4)$$

though we emphasise that this is not a sufficient condition. Our interpretation of (5.4) is that the system cannot be hyperbolic if the total transverse velocity difference all three layers becomes large enough thaat least one of the adjacent transverse velocity differences, $v_1' - v_2'$ or $v_2' - v_3'$, must be large enough to exceed the two-layer critical velocity (4.23).

Except in a few special cases, the quantities defined in (4.5) for the quartic (5.2) are not analytically tractable. Instead, we compute the nature of the roots for a range of velocity differences between adjacent layers. Following (4.18), we define U_1' and U_2' by

$$u_{i+1}' - u_i' = U_i'\cos\psi_i, \qquad v_{i+1}' - v_i' = U_i'\sin\psi_i, \quad (5.5)$$

for $i = 1, 2$, where ψ_i are the orientations of the velocity differences relative to the orientation θ of the axes. The absolute orientations of the velocity differences relative to East are given by $\Psi_i = \theta + \psi_i$.

In figure 4 we illustrate the dependence of the hyperbolicity on U_1' and U_2' in the case of equal layer depths ($h_1 = h_2 = h_3 = 1/3$). Under the traditional approximation ($\tilde{\varepsilon} = 0$), the quartic (5.2) depends only on the parallel velocity differences $u_2' - u_1'$ and $u_3' - u_2'$, so in figure 4(a) we shade regions of $(u_2' - u_1', u_3' - u_2')$ space according to the number of real roots. The result closely resembles figure 3 of Chumakova *et al.* (2009*b*), showing the domain of hyperbolicity for the vertically-periodic non-rotating Boussinesq shallow water equations for three layers of equal depth. Figure 4(b) shows the corresponding result for the very large value $\tilde{\varepsilon} = 2$ of the non-traditional parameter. The domain of hyperbolicity then depends on the full vector velocity differences $\boldsymbol{u}_2' - \boldsymbol{u}_1'$ and $\boldsymbol{u}_3' - \boldsymbol{u}_2'$. The plot is shaded black only when all four eigenvalues are real for all orientations Ψ_1 and Ψ_2 of the velocity shear, and for all directions θ of wave propagation. When alternative values of $\tilde{\varepsilon}$ are used, there is no discernible change in the shaded regions shown in figure 4(b). This includes the traditional case $\tilde{\varepsilon} = 0$. Figure 4(a) would be identical to figure 4(b) if the domain of hyperbolicity were calculated over all Ψ_1, Ψ_2, θ.

In §4 we found that the Boussinesq two-layer shallow water equations lose hyperbolicity when $U' > \sqrt{h_1 + h_2} = 1$. We might therefore expect the three-layer equations to lose hyperbolicity when

$$\hat{U}_1 = \frac{U_1'}{\sqrt{h_1+h_2}} > 1, \quad \text{or} \quad \hat{U}_2 = \frac{U_2'}{\sqrt{h_2+h_3}} > 1, \quad (5.6)$$

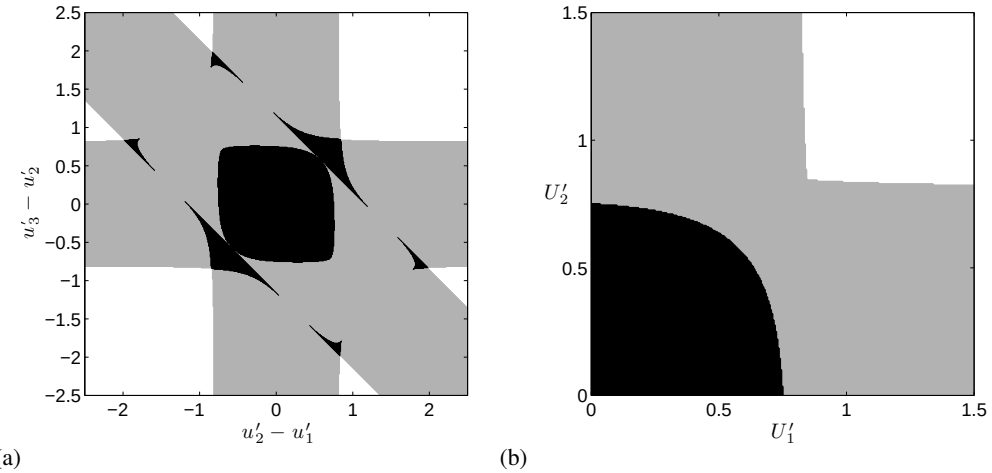

(a) (b)

FIGURE 4. Hyperbolicity of the three-layer shallow water equations over a range of velocity differences between the upper two layers and between the lower two layers: (a) under the traditional approximation $\tilde{\varepsilon} = 0$; (b) for the very large value $\tilde{\varepsilon} = 2$. In (a) the hyperbolicity depends only on $u_2' - u_1'$ and $u_3' - u_2'$. White regions indicate that (5.2) has no real roots, grey regions indicate two real roots, and black regions indicate four real roots. In (b) black regions indicate that (5.2) has four real roots for all values of Ψ_1, Ψ_2 and θ; grey regions indicate at least two real roots for all Ψ_1,Ψ_2 and θ; white regions indicate that there are no real roots for at least one combination of Ψ_1,Ψ_2 and θ.

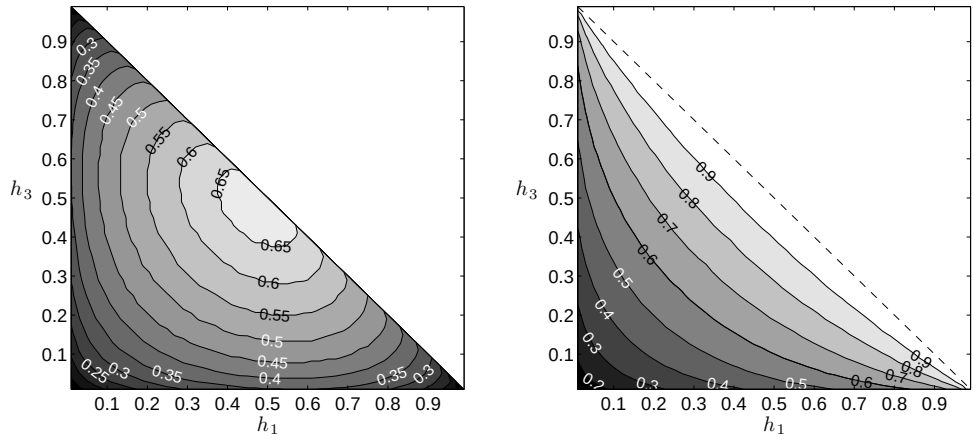

(a) (b)

FIGURE 5. Plots of (a) the largest shear U_c' and (b) the largest scaled shear $\hat{U}_c$, in either layer, for which the three-layer equations are hyperbolic. The plots are restricted to the lower-left triangles by the constraint $h_1 + h_2 + h_3 = 1$.

i.e. when the velocity difference exceeds the internal wave speed defined using the depths of two adjacent layers. Expressing the first condition using the original dimensional variables gives the instability condition

$$\hat{U}_1^2 = \left(\frac{|\tilde{\boldsymbol{u}}_2 - \tilde{\boldsymbol{u}}_1|}{\tilde{h}_1 + \tilde{h}_2} \right)^2 \left(\frac{\sigma g}{\tilde{h}_1 + \tilde{h}_2} \right)^{-1} > 1 \tag{5.7}$$

This expression coincides with the combination of parameters found by Goldstein (1931) to determine the stability of a continuous shear flow in a stratified fluid. In more recent treatments the finite density and velocity differences over a finite distance, here $\tilde{h}_1 + \tilde{h}_2$, are replaced by gradients in the inverse Richardson number

$$\mathrm{Ri}^{-1} = \left| \frac{\partial \tilde{\boldsymbol{u}}}{\partial \tilde{z}} \right|^2 N^{-2} = \left| \frac{\partial \tilde{\boldsymbol{u}}}{\partial \tilde{z}} \right|^2 \left(-\frac{g}{\rho_0} \frac{\partial \tilde{\rho}}{\partial \tilde{z}} \right)^{-1}. \tag{5.8}$$

The quantities $\hat{U}_1^2$ and $\hat{U}_2^2$ may thus be thought of as discrete inverse Richardson numbers.

Equation (5.6) holds exactly in the limit of vanishing middle-layer thickness ($h_2 \to 0$) under the traditional approximation ($\varepsilon = 0$) as the discriminant $\mathcal{D}$ of (5.2) vanishes at these points. This indicates that $\hat{U}_1$ and $\hat{U}_2$ are the most natural variables to describe the loss of hyperbolicity due to shear. Figure 4(b) shows that in general the hyperbolicity does not depend on $\hat{U}_1$ and $\hat{U}_2$ independently, as (5.6) suggests. Rather, its dependence on the upper shear U_1' is influenced by the lower shear U_2', and vice versa.

In figure 5 we quantify the largest velocity differences for which (5.2) is hyperbolic over a range of h_1 and h_3. We may

take $h_1 + h_2 + h_3 = 1$ without loss of generality, by defining the height scale $H = \tilde{h}_1 + \tilde{h}_2 + \tilde{h}_3$. We define U_c' as the largest velocity difference such that the quartic (5.2) has four real roots for all $U_1', U_2' \leqslant U_c'$, and similarly define $\hat{U}_c$ for the rescaled velocity differences $\hat{U}_1$ and $\hat{U}_2$. We plot U_c' and $\hat{U}_c$ for $\varepsilon = 1$ in figures 5(a) and 5(b) respectively. Performing these calculations under the traditional approximation ($\varepsilon = 0$) yields almost identical results: the largest pointwise changes in U_c' and $\hat{U}_c$ are on the order of 10^{-3}. This lies below the precision of the calculations used to create the figures, as indicated by the small undulations in the contour lines in figure 5.

Figure 5(a) shows that U_c' has minima where the thicknesses of any two layers approach zero. Intuitively, as $h_1 + h_2 \to 0$, the squared buoyancy frequency $N^2 \sim (h_1 + h_2)^{-1}$ increases in (5.7), but for a fixed velocity difference the squared shear $|\partial\tilde{\boldsymbol{u}}/\partial\tilde{z}|^2 \sim (h_1 + h_2)^{-2}$ increases more rapidly. Thus U_c' must decrease in order to prevent Ri^{-1} from becoming very large. However, U_c' remains finite as $h_1 + h_2 \to 0$, with a minimum over the entire parameter space of around 0.1. It may appear surprising that U_c' has a maximum of $1/\sqrt{2}$ as $h_2 \to 0$ and $h_1 \to h_3$. However, figure 5(b) shows that this actually the only portion of parameter space in which the expected condition (5.6) describes the hyperbolicity. More surprising is that the discrete inverse Richardson numbers $\hat{U}_1$ and $\hat{U}_2$ must be small as $h_1, h_3 \to 0$, though again $\hat{U}_c$ remains finite in this limit with a minimum of approximately 0.1. We conclude that the three-layer equations become more prone to loss of hyperbolicity when the depth of the uppermost or lowermost layers is reduced, and become comparatively insensitive to loss of hyperbolicity when the depth of the middle layer is reduced.

6. Interpretation as an inertial instability to transverse shear

In this section we relate our criteria for loss of hyperbolicity in our layered models to a condition for the onset of instability in a continuously stratified fluid. The classic baroclinic instability scenario considers a steady state with tilted density surfaces in which the resulting horizontal pressure gradient is balanced by the Coriolis force due to a shear flow. This problem was originally studied by Charney (1947) and Eady (1949) in an atmospheric context, with the tilted density surfaces modelling a background temperature gradient from pole to equator. These studies all considered only disturbances with a wavevector parallel to the background flow, and the resulting unstable motions lie within the quasigeostrophic regime. However, the same configuration is also unstable to ageostrophic perturbations with a wavevector perpendicular to the background flow. This is known as a symmetric instability in the meteorological literature (Fjørtoft 1950; Kuo 1954) since the disturbances are symmetric in the direction of the background flow, but it is equivalent to an inertial instability as seen in a rotating frame, a link that we make precise below. Stone (1966, 1971) relaxed the earlier assumption of hydrostatic balance, identifying the competing regimes of baroclinic, symmetric, and Kelvin–Helmholtz instabilities in a single analysis. Jeffery & Wingate (2009) and Colin de Verdière (2012) recently revisited this problem with the complete Corolis force, improving upon the work of Hathaway *et al.* (1979) and Sun (1995) who included the complete Coriolis force in the evolution of the perturbations, but not for determining the background state. Hua *et al.* (1997) had previously studied symmetric instabilities on an equatorial β-plane, showing that the criterion for the onset of instability remains negative Ertel potential vorticity, as modified by the inclusion of the full rotation vector.

6.1. *Three-dimensional non-traditional Boussinesq equations*

We consider the three-dimensional Boussinesq equations for a continuously stratified fluid whose density $\rho = \rho_0 + \tilde{\rho}$ makes small excursions $\tilde{\rho}$ from a constant background density ρ_0 (*e.g.* Vallis 2006)

$$\mathrm{D}_t\boldsymbol{u} + 2\boldsymbol{\Omega} \times \boldsymbol{u} + \nabla\Phi = b\hat{\boldsymbol{z}}, \tag{6.1a}$$

$$\nabla \cdot \boldsymbol{u} = 0, \tag{6.1b}$$

$$\mathrm{D}_t b = 0, \tag{6.1c}$$

where $\mathrm{D}_t = \partial/\partial t + \boldsymbol{u} \cdot \nabla$ is the material time derivative for the three-dimensional velocity field $\boldsymbol{u} = (u, v, w)$, and $\boldsymbol{\Omega} = (\Omega_x, \Omega_y, \Omega_z)$ is the three-dimensional rotation vector. As in §2, we assume the horizontal scales are sufficiently short that $\boldsymbol{\Omega}$ may be treated as a constant. We write the total pressure as $p = p_0 + \rho_0\Phi$, where $p_0(z)$ is in hydrostatic balance with the background density, $\mathrm{d}p_0/\mathrm{d}z = -g\rho_0$. Pressure perturbations from this background are represented by the geopotential Φ, and density perturbations by the buoyancy $b = -g\tilde{\rho}/\rho_0$. All quantities are dimensional.

We first consider a steady solution of (6.1*a*)–(6.1*c*), denoted by a superscript star *, in which the velocity is purely in the x direction, and $u^\star$ and $b^\star$ both vary linearly with depth,

$$u^\star = zU_z, \quad b^\star = zN^2 - 2y\Omega_z U_z. \tag{6.2}$$

The background shear requires constant buoyancy surfaces (isopycnals) that are tilted in the yz plane to satisfy non-traditional geostrophic (*e.g.* Hua *et al.* 1997) and quasihydrostatic balance relative to the geopotential

$$\Phi^\star = \tfrac{1}{2}z^2\left(N^2 + 2\Omega_y U_z\right) - 2\,yz\,\Omega_z U_z. \tag{6.3}$$

These conditions together make up the non-traditional thermal wind balance. The Brunt–Väisälä frequency $N = \sqrt{-(g/\rho_0)\partial\tilde{\rho}/\partial z}$ and the background velocity shear $U_z = \mathrm{d}u^\star/\mathrm{d}z$ are both constants.

We now consider small, time-dependent perturbations to this steady solution,

$$u = u^\star + u', \quad v = v', \quad w = w', \quad b = b^\star + b', \quad \Phi = \Phi^\star + \Phi', \tag{6.4}$$

where primes $'$ denote small perturbations. For simplicity we restrict our attention to waves propagating along the y-axis, and neglect all derivatives with respect to x. Although it differs from earlier sections, this choice of axes lets us study symmetric instabilitities in the standard axes of geophysical fluid dynamics with x directed due east. Linearising (6.1*a*)–(6.1*c*) in the perturbations (6.4) yields

$$\frac{\partial u'}{\partial t} + w'U_z - 2\Omega_z v' + 2\Omega_y w' = 0, \tag{6.5a}$$

$$\frac{\partial v'}{\partial t} + 2\Omega_z u' - 2\Omega_x w' + \frac{\partial \Phi'}{\partial y} = 0, \tag{6.5b}$$

$$\frac{\partial w'}{\partial t} + 2\Omega_x v' - 2\Omega_y u' + \frac{\partial \Phi'}{\partial z} = b', \tag{6.5c}$$

$$\frac{\partial v'}{\partial y} + \frac{\partial w'}{\partial z} = 0, \tag{6.5d}$$

$$\frac{\partial b'}{\partial t} - 2\Omega_z U_z v' + N^2 w' = 0. \tag{6.5e}$$

6.2. *Uniform oscillations at the equator*

We first consider spatially-uniform solutions of (6.5*a*)–(6.5*e*), and restrict our attention to the equator ($\phi = 0$) to remove the influence of Ω_z and highlight the influence of the non-traditional components of the Coriolis force. Under these assumptions, (6.5*a*)–(6.5*e*) may be rearranged into a single equation for the vertical velocity,

$$\partial_{tt} w' + N_\mathrm{e}^2 w' = 0, \quad \text{where} \quad N_\mathrm{e}^2 = N^2 + 4(\Omega_x^2 + \Omega_y^2) + 2U_z\Omega_y. \tag{6.6}$$

This equation describes oscillations with an effective buoyancy frequency N_e that is modified by the inclusion of the complete Coriolis force. It corresponds to the non-traditional form of the Eliassen–Sawyer equation (Eliassen 1951; Sawyer 1949) given by Hua *et al.* (1997) for meridional streamfunctions that depends only upon y. The effective buoyancy frequency N_e reduces to the Brunt–Väisälä frequency N under the traditional approximation ($\Omega_x = \Omega_y = 0$).

In the absence of a background velocity shear ($U_z = 0$), the complete Coriolis force increases the effective buoyancy frequency through the strictly positive terms $4(\Omega_x^2 + \Omega_y^2)$. This may be most easily understood for eastward-propagating waves, so we choose axes in which y points eastward, and x points southward. The horizontal components of the rotation vector are then $\Omega_x = -\Omega$ and $\Omega_y = 0$. A positive vertical velocity perturbation w' accelerates a westward horizontal velocity perturbation v' via the zonal momentum equation (6.5*b*). This in turn induces a negative vertical acceleration via the vertical momentum equation (6.5*c*). Thus the non-traditional components of the Coriolis force due to Ω_x tend to stabilise small vertical perturbations.

By contrast, a non-zero background velocity shear ($U_z \neq 0$) reduces the effective buoyancy frequency N_e when the product $U_z\Omega_y$ is negative. Without loss of generality we restrict our attention to axes in which the x-axis is directed eastward rather than westward, and the y-axis is directed northward so that $\Omega_y > 0$. This restricts the angle θ to $|\theta| < \pi/2$. A shear with $U_z < 0$ describes a flow whose westward velocity increases with increasing height z. This reduces the effective buoyancy frequency N_e. For sufficiently large and negative U_z the effective buoyancy frequency N_e becomes complex, so fluid parcels are unstable to infinitesimal vertical perturbations. More precisely, the flow becomes unstable when

$$-U_z > \frac{N^2 + 4\Omega_x^2 + 4\Omega_y^2}{2\Omega_y}, \tag{6.7}$$

which is analogous to the instability criteria (4.24) and (5.4) for transverse shear in the two- and three-layer shallow water equations.

To interpret (6.7) physically, we adopt the standard axes of geophysical fluid dynamics with the x-axis pointing due east, and the y-axis pointing due north, so $\Omega_x = 0$ and $\Omega_y = \Omega$. We rewrite condition (6.7) as

$$-2\Omega(U_z + 2\Omega) > N^2 \quad \Longrightarrow \quad -2\Omega\frac{\mathrm{d}u_\mathrm{a}^\star}{\mathrm{d}z} > N^2, \quad u_\mathrm{a}^\star = 2\Omega z + u^\star. \tag{6.8}$$

Here $u_\mathrm{a}^\star$ is the total zonal angular momentum, whose origin is explained under (6.15) below. A necessary condition for instability is thus $\mathrm{d}u_\mathrm{a}^\star/\mathrm{d}z < 0$. Hoskins (1974) interpreted this condition as a stratified version of Rayleigh's (1917) criterion for a homogeneous rotating fluid being unstable if its angular momentum decreases with distance from the axis of rotation.

When $\mathrm{d}u_{\mathrm{a}}^{\star}/\mathrm{d}z < 0$, a positive vertical velocity perturbation w' induces a westward acceleration via the zonal momentum equation (6.5*a*), and the resulting positive velocity v' induces an even larger positive vertical velocity via (6.5*c*). There is thus a positive feedback between the zonal acceleration by the background angular momentum in (6.5*a*) and the vertical acceleration by the non-traditional component of the Coriolis force in (6.5*c*). Condition (6.8) simply states that the flow is unstable to infinitesimal vertical perturbations when this positive feedback exceeds the restoring force due to the background stratification. Writing the conditions (6.7) and (6.8) as

$$\left(-\frac{g}{\rho_0}\frac{\partial \rho}{\partial z}\right) + 4(\Omega_x^2 + \Omega_y^2) < -2\Omega_y U_z \tag{6.9}$$

suggests an analogy with the condition for loss of hyperbolicity due to the Eötvös effect in the single layer non-traditional shallow water equations (Dellar & Salmon 2005)

$$g < 2(\Omega_x^2 + \Omega_y^2)^{1/2}|\boldsymbol{u}|. \tag{6.10}$$

The appearance of vertical gradients in (6.9) suggests an interpretation as loss of stability due to a vertical gradient in the Eötvös effect caused by the vertical gradient in the zonal velocity. A fluid particle displaced vertically experiences a change in the upward force due to the Eötvös effect that exceeds the restoring force due to density stratification.

6.3. *Plane-wave solutions*

Our analysis in §6.2 demonstrates that a vertical shear in the horizontal velocity may destabilise the flow via the action of the non-traditional components of the Coriolis force. However, we restricted our attention to a very specific scenario for the purpose of illustration. We now allow a non-zero latitude ($\phi \neq 0$) and allow the perturbed variables to depend upon both y and z. We seek plane wave solutions of the form

$$b'(y,z,t) = \hat{b}\, e^{i(ky+mz-\omega t)}, \tag{6.11}$$

where ω is the wave frequency and k and m are the horizontal and vertical wave numbers respectively. Substituting (6.11) into (6.5*a*)–(6.5*e*) yields the dispersion relation

$$\omega^2 = \frac{1}{1+K^2}\left(N^2 + \left(2\Omega_z K + 2\Omega_y\right)^2 + 2\Omega_y U_z + 4\Omega_z U_z K\right), \tag{6.12}$$

where $K = m/k$ is the ratio of the vertical to horizontal wave numbers. The component Ω_x does not appear in (6.12), consistent with the analogous results in §4 and §5. However, the background shear U_z appears in (6.12) through the combinations $2\Omega_y U_z$ and $4\Omega_z U_z K$, so shear may destabilise the flow via either of the other components of the rotation vector.

Colin de Verdière (2012) gave an equivalent dispersion relation, which is the non-traditional extension of dispersion relations given by Ooyama (1966); Hoskins (1974); Mooers (1975) and Xui & Clark (1985). Sun (1995) found a similar dispersion relation that included some non-traditional terms, but the coefficients were different due to the neglect of non-traditional effects in calculating the basic state. Seeking plane wave solutions of an equation in Jeffery & Wingate (2009) leads to (6.12) without the $2\Omega_y U_z$ term. Their background state differs from ours through the inclusion of a term proportional to $2\Omega_y U_z$ in the buoyancy, which becomes $b^{\star} = z(N^2 - 2\Omega_y U_z) - 2y\Omega_z U_z$, and its omissions from the geopotential, which becomes $\Phi^{\star} = \frac{1}{2}z^2 N^2 - 2\,yz\,\Omega_z U_z$. Equivalently, they replaced our N^2 with $N^2 - 2\Omega_y U_z$ in (6.2) and (6.3), and hence also in (6.12).

The dispersion relation (6.12) has two recognisable limits. For purely vertical wave propagation, it gives inertial oscillations with frequency

$$\omega = \pm 2\Omega_z, \tag{6.13}$$

which corresponds to the limit $|K| \to \infty$. In the opposite limit $K \to 0$, corresponding to purely horizontal propagation, (6.12) reduces to

$$\omega^2 = N^2 + 4\Omega_y^2 + 2\Omega_y U_z. \tag{6.14}$$

In this case the wave frequency ω coincides with the effective buoyancy frequency (6.6) for uniform oscillations at the equator, except omitting the x-dependence while retaining the y dependence eliminates Ω_x from (6.12) and hence from its limiting form (6.14). The corresponding instability criterion

$$-U_z > \frac{N^2 + 4\Omega_y^2}{2\Omega_y}, \tag{6.15}$$

may be interpreted using (6.8) for the total angular momentum $u_{\mathrm{a}}^{\star} = 2(z\Omega_y - y\Omega_z) + u^{\star}$ with a contribution from the traditional Coriolis force. This expression comes from the x-component of $\boldsymbol{u}_{\mathrm{a}}^{\star} = \boldsymbol{u}^{\star} + \boldsymbol{R}$, where $\boldsymbol{R} = (2z\Omega_y - 2y\Omega_z, -z\Omega_x - x\Omega_z, y\Omega_x + x\Omega_y)$ is a vector potential for the Coriolis force satisfying $\nabla \times \boldsymbol{R} = 2\boldsymbol{\Omega}$ with R_x having no explicit x-dependence. Conservation of $u_{\mathrm{a}}^{\star}$ in the absence of pressure torques then follows from the translational symmetry in x via Noether's theorem (*e.g.* Dellar & Salmon 2005).

Condition (6.15) is also analogous to the criteria (4.24) and (5.4) for ill-posedness due to transverse shear in the two- and three-layer shallow-water equations. In particular, the dimensional equivalent of (4.24) in rotated axes is

$$-\frac{\tilde{u}_1 - \tilde{u}_2}{\Delta H} > \frac{N_{\rm sw}^2 + 2\Omega_y^2}{2\Omega_y}, \quad \text{where} \quad N_{\rm sw}^2 = \frac{g}{\rho_2}\frac{(\rho_2 - \rho_1)}{\Delta H}. \tag{6.16}$$

We use $\Delta H = H/2$ as the distance between the mid-surfaces of the two undisturbed layers, and interpret ratios with ΔH as discrete analogues of the derivatives $\partial_z \tilde{u}$ and $\partial_z \rho$. For example, we interpret $N_{\rm sw}$ as an effective buoyancy frequency for the shallow water equations. Conditions (6.15) and (6.16) differ only by the factor of 2 or 4 multiplying the Ω_y^2 term in the numerator. The small aspect ratio expansion used to derive the non-traditional shallow water equations leads to vertical velocities that are linear in z (Dellar & Salmon 2005; Stewart & Dellar 2010). The depth average of terms linear in the vertical velocities is thus equal to the value of these terms at the mid-surfaces, but this result does not hold for the products of non-traditional terms that set the basis state.

More generally, waves propagating in an arbitrary direction (k, m) are unstable if the ω^2 given by (6.12) is negative for any real K. The bracketed expression on the right-hand side of (6.12) is quadratic in K, and has two roots when

$$\Omega_z^2 \left(U_z^2 + 2\Omega_y U_z - N^2 \right) > 0. \tag{6.17}$$

For Ω_z non-zero, the flow is thus unstable for a finite range of wave numbers when

$$|U_z + \Omega_y| > \sqrt{N^2 + \Omega_y^2}. \tag{6.18}$$

This condition for instability coincides with the negative non-traditional Ertel potential vorticity condition $\Omega_z Q_E \leqslant 0$ of Hua *et al.* (1997) for $Q_E = (2\boldsymbol{\Omega} + \nabla \times \boldsymbol{u}) \cdot \nabla b$. The latter is the non-traditional version of Hoskins's (1974) generalisation of the Rayleigh (1917) criterion to rotating frames, and identifies the instability as a conventional symmetric or inertial instability involving the traditional part of the Coriolis force. By contrast, the instability described by (6.15) in the limit $K \to 0$ leads to a loss of hyperbolicity in the multilayer shallow water equations, suggesting that it has the character of a shear instability driven by the non-traditional components of the Coriolis force. Hua *et al.* (1997) found that the the time-averaged zonal velocity $\overline{u}$ from PEQUOD ocean data approximately follows $\overline{u} = -2\Omega z$, with z being depth below the surface. This relation corresponds to vanishing non-traditional Ertel potential vorticity Q_E, suggesting that the conditions for the onset of non-traditional transverse shear instability may also be met in weakly stratified regions of the abyssal ocean where $N \lesssim \Omega$.

7. Conclusion

We have analysed the hyperbolicity of multilayer shallow water equations that include the complete Coriolis force, as derived in our earlier paper (Stewart & Dellar 2010). Multilayer shallow water theory assumes that the horizontal fluid velocity is approximately uniform within each layer, with differences concentrated into vortex sheets at the interfaces between layers. This configuration leads to Kelvin–Helmholtz instabilities in the three-dimensional Euler equations, with growth rates proportional to the wavenumber k of the disturbance. These instabilities manifest themselves in shallow water theory through a loss of hyperbolicity of the shallow water equations, which thus become ill-posed for initial value problems.

The traditional multilayer shallow water equations are derived under the hydrostatic approximation. This tames the Kelvin–Helmholtz instability to the extent that it may be completely stabilised at all wavenumbers by sufficiently strong stratification. In particular, the two-layer shallow water equations remain hyperbolic when the velocity difference between the layers is smaller than twice the internal wave speed, the relevant measure of the strength of the stratification (Long 1956; Liska & Wendroff 1997). Conversely, the multilayer Green–Naghdi (1976) equations that retain the vertical acceleration are ill-posed for any non-zero velocity difference between adjacent layers (Liska & Wendroff 1997). Our non-traditional multilayer water equations are derived under the "quasi-hydrostatic" approximation (White & Bromley 1995) that retains the vertical component of the Coriolis force, but still neglects the vertical acceleration.

In §4 we focused on the two-layer non-traditional shallow water equations because they are the most analytically tractable. We rescaled the equations by the internal gravity wave speed and internal deformation radius, and calculated the velocity differences under which they remain hyperbolic in the limit of a small relative density difference between the layers, $\sigma = 1 - \rho_1/\rho_2 \ll 1$. Figure 2 shows that this provides a very good approximation to the actual hyperbolicity condition even when $\sigma = O(1)$. To leading order in σ, the threshold magnitude for velocity difference (in any direction) below which the equations remain hyperbolic is the same for both the traditional and non-traditional equations. However, the traditional shallow water equations only lose hyperbolicity through velocity differences parallel to the wavevector of the disturbances. Including the complete Coriolis force also leads to loss of hyperbolicity due to transverse velocity differences. The vertical lines in figure 2 marking the domain of hyperbolicity under the traditional approximation thus become curves when non-traditional effects are included. The complete Coriolis force also causes an additional loss of hyperbolicity when the eastward velocity in either layer is sufficiently large, as shown in figure 3. This represents an extreme form of the Eötvös effect (*e.g.* Persson 2005) that

would not arise for any geophysically realistic fluid velocity. However, the loss of hyperbolicity due to transverse velocity difference may also be interpreted as due to a gradient Eötvös effect overcoming weak stratification, which is geophysically relevant in the deep ocean.

For more than two layers, the hyperbolicity analysis quickly becomes intractable, so in §5 we computed the hyperbolicity domain of the three-layer equations numerically, again under the assumption of small σ. We demonstrated that, in the case of equal density differences and equal layer depths, the threshold for the velocity differences between adjacent layers under which the equations remain hyperbolic is unchanged by the inclusion of the complete Coriolis force. However, the shape of the domain of hyperbolicity outside this threshold changes substantially. Our findings are encouraging in that the non-traditional shallow water equations are well-posed for initial value problems when the velocity differences between layers are smaller than the characteristic internal wave speed, just as for the traditional shallow water equations. This makes our equations a viable model for various non-traditional phenomena in geophysical fluid dynamics (see *e.g.* Gerkema *et al.* 2008) and a viable basis for including the non-traditional Coriolis terms in predictive numerical ocean models such as MICOM and GOLD.

In §6 we interpreted our results using the dispersion relation for perturbations in the continuously stratified Boussinesq equations linearised about a velocity shear perpendicular to the direction of wave propagation, as found recently by Colin de Verdière (2012). Our criteria for loss of hyperbolicity due to transverse velocity differences in our multilayer shallow water equations are natural discrete analogues of a criterion for the onset of a non-traditional inertial instability in the continuously stratified equations. This provides another example of the correspondence between loss of well-posedness and instability found by Chumakova *et al.* (2009*a*,*b*) for non-rotating stratified shear flows and their shallow water analogues. The non-traditional component of the Coriolis force stabilises vertical perturbations for zero velocity shear, and may either stabilise or de-stabilise perturbations when the velocity shear is non-zero. The same calculation demonstrates that the non-traditional component of the Coriolis force modifies the range of unstable wave numbers, the most unstable wave number, and the maximum growth rate of the instability. One might expect this instability to be important in weakly stratified parts of the ocean where the buoyancy frequency N is comparable to or smaller than the inertial frequency. These include the deep Mediterranean (van Haren & Millot 2005), the Southern Ocean (Heywood *et al.* 2002) and the Labrador Sea (Lazier 1980), so this instability may have implications for mixing in the abyssal ocean, and for sub-mesoscale processes in the surface mixed layer. However, for simplicity we restricted our attention to waves propagating perpendicular to the velocity shear, following the standard treatment of symmetric instabilities under the traditional approximation. A full analysis of the influence of the complete Coriolis force on inertial instabilities must allow for propagation in all directions.

This work was supported by the Engineering and Physical Sciences Research Council through a PhD Plus award to A.L.S. and an Advanced Research Fellowship [grant number EP/E054625/1] to P.J.D.

Appendix A. Matrices for the quasilinear form of the two-layer equations

The matrix of coefficients $\mathbf{C}_x$ and vector of algebraic terms $\boldsymbol{b}$ that appear in (3.1), the quasilinear form of the multilayer shallow water equations, are

$$\mathbf{C}_x = \begin{bmatrix} u_1 - \varepsilon\, h_1\Omega_y & \frac{1}{2}\,\varepsilon\, h_1\Omega_x & 1 + \varepsilon\,(v_1\,\Omega_x - u_1\,\Omega_y) \\ \frac{1}{2}\,\varepsilon\, h_1\Omega_x & u_1 & 0 \\ h_1 & 0 & u_1 \\ -\varepsilon(1-\sigma)\, h_1\Omega_y & \varepsilon(1-\sigma)\, h_1\Omega_x & (1-\sigma)\,[1 + \varepsilon\,(v_1\Omega_x - u_1\Omega_y)] \\ 0 & 0 & 0 \\ 0 & 0 & 0 \end{bmatrix}$$

$$\begin{bmatrix} -\varepsilon\, h_2\,\Omega_x & 0 & 1 + \varepsilon\,(v_1\,\Omega_x - u_2\,\Omega_y) \\ \varepsilon\, h_2\,\Omega_x & 0 & \varepsilon\,(u_2 - u_1)\,\Omega_x \\ 0 & 0 & 0 \\ u_2 - \varepsilon\, h_2\,\Omega_y & \frac{1}{2}\,\varepsilon\, h_2\,\Omega_x & 1 + \varepsilon\,(v_2\,\Omega_x - u_2\,\Omega_y) \\ \frac{1}{2}\,\varepsilon\, h_2\,\Omega_x & u_2 & 0 \\ h_2 & 0 & u_2 \end{bmatrix}, \tag{A 1}$$

$$\boldsymbol{b} = \begin{bmatrix} \dfrac{\partial h_b}{\partial x} - (\Omega_z - \varepsilon \boldsymbol{\Omega} \cdot \nabla h_b)\, v_1 \\ \dfrac{\partial h_b}{\partial y} + (\Omega_z - \varepsilon \boldsymbol{\Omega} \cdot \nabla h_b)\, u_1 \\ 0 \\ \dfrac{\partial h_b}{\partial x} - (\Omega_z - \varepsilon \boldsymbol{\Omega} \cdot \nabla h_b)\, v_2 \\ \dfrac{\partial h_b}{\partial y} + (\Omega_z - \varepsilon \boldsymbol{\Omega} \cdot \nabla h_b)\, u_2 \\ 0 \end{bmatrix}. \tag{A 2}$$

Here $\sigma = 1 - \rho_1/\rho_2$ is the relative density difference, and subscripts $_1$ and $_2$ correspond to the upper and lower layers respectively.

Appendix B. Quartic polynomial for hyperbolicity of the two-layer equations

The two-layer shallow water equations, discussed in §4, are hyperbolic when all roots of the following polynomial in λ are real for all orientations θ of the x and y axes,

$$\begin{aligned} &\lambda^4 + \Big[\varepsilon\, \Omega_y(h_1 + h_2) - 2(u_1 + u_2)\Big]\, \lambda^3 \\ &\quad + \Big[\, u_1^2 + u_2^2 + 4\, u_2 u_1 - h_2 - h_1 \\ &\qquad - (2\, \Omega_y(u_2 h_1 + u_1 h_2) + \Omega_x(h_1 v_1 + h_2 v_2))\, \varepsilon \\ &\qquad\quad + \left(h_1 h_2(\sigma(\Omega_x^2 + \Omega_y^2) - \frac{1}{4}\Omega_x^2) - \Omega_x^2(h_1^2 + h_2^2)\right) \varepsilon^2 \,\Big]\, \lambda^2 \\ &\quad + \Big[\, 2(u_1 h_2 + u_2 h_2 - u_1 u_2(u_1 + u_2)) - \frac{1}{4}\, h_1 h_2 \Omega_y \Omega_x^2 (h_1 + h_2)\varepsilon^3 \\ &\qquad + \left(\Omega_x^2 \left(\frac{1}{2} u_1 h_2^2 + \frac{1}{2} u_2 h_1^2 + 2 u_1 h_1 h_2 (1 - \sigma)\right) + \Omega_x \Omega_y h_1 h_2\, ((1 - 2\sigma) v_1 - v_2)\right) \varepsilon^2 \\ &\qquad\quad + \left(2\Omega_x\, (u_1 h_2 v_2 + u_2 h_1 v_1) + \Omega_y \left(u_1^2 h_2 + u_2^2 h_1 - 2\sigma h_1 h_2\right)\right) \varepsilon \,\Big]\, \lambda \\ &\quad + \Big[\, \frac{1}{4} \Omega_x^3 h_1 h_2\, (h_2 v_1 + h_1 v_2)\, \varepsilon^3 + \left(u_1^2 u_2^2 - h_1 u_2^2 - h_2 u_1^2 + \sigma h_1 h_2\right) \\ &\qquad + \frac{1}{4} \Omega_x^2 \left(h_1 h_2 \left(h_1 + h_2 + 4 v_1 v_2 - 4(1 - \sigma) \left(u_1^2 + v_1^2\right)\right) - h_1^2 u_2^2 - h_2^2 u_1^2\right) \varepsilon^2 \\ &\qquad\quad + \Omega_x \left(h_1 h_1\, (v_2 + (2\sigma - 1) v_1) - h_1 v_1 u_2^2 - h_2 v_2 u_1^2\right) \varepsilon + \frac{1}{16} h_1^2 h_2^2 \Omega_x^4 \varepsilon^4 \,\Big] = 0. \end{aligned} \tag{B 1}$$

REFERENCES

ABRAMOWITZ, M. & STEGUN, I. A. 1965 *Handbook of Mathematical Functions*. Dover.

ADCROFT, A. & HALLBERG, R. 2006 On methods for solving the oceanic equations of motion in generalized vertical coordinates. *Ocean Model.* **11**, 224–233.

BENZONI-GAVAGE, S. & SERRE, D. 2007 *Multi-Dimensional Hyperbolic Partial Differential Equations: First Order Systems and Applications*. Oxford University Press.

BLECK, R. & CHASSIGNET, E. 1994 Simulating the oceanic circulation with isopycnic-coordinate models. In *The Oceans: Physical-Chemical Dynamics and Human Impact* (ed. S.K. Majumdar, E.W. Miller, G.S. Forbe, R.F. Schmalz & A.A. Panah), pp. 17–39. Pennsylvania Acad. Sci.

BLECK, R., ROOTH, C., HU, D. & SMITH, L. T. 1992 Salinity-driven thermocline transients in a wind- and thermohaline-forced isopycnic coordinate model of the North Atlantic. *J. Phys. Oceanogr.* **22**, 1486–1505.

BOSS, E., PALDOR, N. & THOMPSON, L. 1996 Stability of a potential vorticity front: From quasi-geostrophy to shallow water. *J. Fluid Mech.* **315**, 65–84.

CHANDRASEKHAR, S. 1961 *Hydrodynamic and Hydromagnetic Stability*. Oxford University Press.

CHARNEY, J. G. 1947 The dynamics of long waves in a baroclinic westerly current. *J. Meteor.* **4**, 136–162.

CHOBOTER, P. F. & SWATERS, G. E. 2004 Shallow water modeling of Antarctic bottom water crossing the equator. *J. Geophys. Res.* **C109**, 03038.

CHUMAKOVA, L., MENZAQUE, F. E., MILEWSKI, P. A., ROSALES, R. R., TABAK, E. G. & TURNER, C. V. 2009*a* Shear instability for stratified hydrostatic flows. *Comm. Pure Appl. Math.* **62**, 183–197.

CHUMAKOVA, L., MENZAQUE, F. E., MILEWSKI, P. A., ROSALES, R. R., TABAK, E. G. & TURNER, C. V. 2009*b* Stability properties and nonlinear mappings of two and three-layer stratified flows. *Stud. Appl. Math.* **122**, 123–137.

COLIN DE VERDIÈRE, A. 2012 The stability of short symmetric internal waves on sloping fronts: Beyond the traditional approximation. *J. Phys. Oceanogr.* **42**, 459–475.

DELLAR, P. J. & SALMON, R. 2005 Shallow water equations with a complete Coriolis force and topography. *Phys. Fluids* **17**, 106601–19.

EADY, E. T. 1949 Long waves and cyclone waves. *Tellus* **1**, 33–52.

ECKART, C. 1960 *Hydrodynamics of Oceans and Atmospheres*. Pergamon.

ELIASSEN, A. 1951 Slow thermally or frictionally controlled meridional circulation in a circular vortex. *Astrophysica Norvegica* **5**, 19–60.

FJØRTOFT, R. 1950 Application of integral theorems in deriving criteria of stability for laminar flows and for the baroclinic circular vortex. *Geofys. publikasjoner* **17**.

FRIEDRICHS, K. O. 1954 Symmetric hyperbolic linear differential equations. *Comm. Pure Appl. Math.* **7**, 345–392.

GARVER, R. 1933 On the nature of the roots of a quartic equation. *Math. News Lett.* **7**, 6–8.

GERKEMA, T. & SHRIRA, V. I. 2005*a* Near-inertial waves in the ocean: beyond the "traditional approximation". *J. Fluid Mech.* **529**, 195–219.

GERKEMA, T. & SHRIRA, V. I. 2005*b* Near-inertial waves on the non-traditional β-plane. *J. Geophys. Res.* **110**, C10003.

GERKEMA, T., ZIMMERMAN, J. T. F., MAAS, L. R. M. & VAN HAREN, H. 2008 Geophysical and astrophysical fluid dynamics beyond the traditional approximation. *Rev. Geophys.* **46**, RG2004.

GILL, A. E. 1982 *Atmosphere Ocean Dynamics*. Academic Press.

GODLEWSKI, E. & RAVIART, P.-A. 1996 *Numerical Approximation of Hyperbolic Systems of Conservation Laws*. Springer.

GOLDSTEIN, S. 1931 On the stability of superposed streams of fluids of different densities. *Proc. R. Soc. Lond. A* **132**, 524–548.

GREEN, A.E. & NAGHDI, P.M. 1976 A derivation of equations for wave propagation in water of variable depth. *J. Fluid Mech.* **78**, 237–246.

HADAMARD, J. 1923 *Lectures on Cauchy's problem in Linear Partial Differential Equations*. Yale University Press.

VAN HAREN, H. & MILLOT, C. 2005 Gyroscopic waves in the Mediterranean Sea. *Geophys. Res. Lett.* **32**, L24614.

HATHAWAY, D. H., GILMAN, P. A. & TOOMRE, JURI 1979 Convective instability when the temperature gradient and rotation vector are oblique to gravity. I. Fluids without diffusion. *Geophys. Astrophys. Fluid Dyn.* **13**, 289–316.

HEYWOOD, K. J., NAVEIRA GARABATO, A. C. & STEVENS, D. P. 2002 High mixing rates in the abyssal Southern Ocean. *Nature* **415**, 1011–1014.

HOSKINS, J. B. 1974 The role of potential vorticity in symmetric stability and instability. *Quart. J. Roy. Met. Soc.* **100**, 480–482.

HOUGHTON, D. & ISAACSON, E. 1970 Mountain winds. In *Numerical Solutions of Nonlinear Problems* (ed. J. M. Ortega & W. C. Rheinboldt), *Studies in Numerical Analysis*, vol. 2, pp. 21–52. Society for Industrial and Applied Mathematics.

HOWARD, L. N. 1961 Note on a paper of John W. Miles. *J. Fluid Mech.* **10**, 509–512.

HUA, B. L., MOORE, D. W. & LE GENTIL, S. 1997 Inertial nonlinear equilibration of equatorial flows. *J. Fluid Mech.* **331**, 345–371.

IRVING, R. S. 2004 *Integers, Polynomials, and Rings*. Springer.

JEFFERY, N. & WINGATE, B. 2009 The effect of tilted rotation on shear instabilities at low stratifications. *J. Phys. Oceanogr.* **39**, 3147–3161.

JOSEPH, D. D. & SAUT, J. C. 1990 Short-wave instabilities and ill-posed initial-value problems. *Theor. Comp. Fluid Dyn.* **1**, 191–227.

KELDER, H. & TEITELBAUM, H. 1991 A note on instabilities of a Kelvin–Helmholtz velocity profile in different approximations. *Il Nuovo Cimento C* **14**, 107–118.

KU, W. 1965 Explicit criterion for the positive definiteness of a general quartic form. *IEEE Trans. Autom. Control* **10**, 372–373.

KUO, H-L. 1954 Symmetrical disturbances in a thin layer of fluid subject to a horizontal temperature gradient and rotation. *J. Met.* **11**, 399–411.

LAMB, H. 1932 *Hydrodynamics*, 6th edn. Cambridge University Press.

LAWRENCE, G. A. 1990 On the hydraulics of Boussinesq and non-Boussinesq two-layer flows. *J. Fluid Mech.* **215**, 457–480.

LAZIER, J. R. N. 1980 Oceanographic conditions at Ocean Weather Ship Bravo, 1964–1974. *Atmosphere-Ocean* **18**, 227–238.

LEBLOND, P. H. & MYSAK, L. A. 1978 *Waves in the Ocean*. Elsevier.

LEIBOVICH, S. & LELE, S. K. 1985 The influence of the horizontal component of Earth's angular velocity on the instability of the Ekman layer. *J. Fluid Mech.* **150**, 41–87.

LISKA, R., MARGOLIN, L. & WENDROFF, B. 1995 Nonhydrostatic two-layer models of incompressible flow. *Comput. Math. Applic.* **29**, 25–37.

LISKA, R. & WENDROFF, B. 1997 Analysis and computation with stratified fluid models. *J. Comput. Phys.* **137**, 212–244.

LONG, R. R. 1956 Long waves in a two-fluid system. *J. Met.* **13**, 70–74.

MARCHAL, O. & NYCANDER, J. 2004 Nonuniform upwelling in a shallow-water model of the Antarctic Bottom Water in the Brazil Basin. *J. Phys. Oceanogr.* **34**, 2492–2513.

MARSHALL, J. & SCHOTT, F. 1999 Open-ocean convection: Observations, theory, and models. *Rev. Geophys.* **37**, 1–64.

MILES, J. W. 1961 On the stability of heterogeneous shear flows. *J. Fluid Mech.* **10**, 496–508.

MOOERS, C. N. K. 1975 Several effects of a baroclinic current on the crossstream propagation of inertial-internal waves. *Geophys. Fluid Dynam.* **6**, 245–275.

OOYAMA, K. 1966 On the stability of the baroclinic circular vortex: a sufficient criterion for instability. *J. Atmos. Sci.* **23**, 43–53.

PEDLOSKY, J. 1987 *Geophysical Fluid Dynamics*, 2nd edn. Springer.

PERSSON, A. 2005 The Coriolis effect: Four centuries of conflict between common sense and mathematics, Part I: A history to 1885. *Hist. Meteorol.* **2**, 1–24.

PHILLIPS, N. A. 1954 Energy transformations and meridional circulations associated with simple baroclinic waves in a two-level, quasi-geostrophic model. *Tellus* **6**, 273–286.

PHILLIPS, N. A. 1968 Reply to Comment by Veronis. *J. Atmos. Sci.* **25**, 1155–1157.

PHILLIPS, N. A. 1973 Principles of large scale numerical weather prediction. In *Dynamic meteorology: Lectures delivered at the Summer School of Space Physics of the Centre National d'Études Spatiales* (ed. P. Morel), pp. 3–96. D. Reidel Pub. Co.

QUENEY, P. 1950 Adiabatic perturbation equations for a zonal atmospheric current. *Tellus* **2**, 35–51.

RAYLEIGH, LORD 1917 On the dynamics of revolving fluids. *Proc. Roy. Soc. Lond. Ser. A* **93**, 148–154.

RENARDY, M. & ROGERS, R. C. 2004 *An Introduction to Partial Differential Equations*, 2nd edn. Springer.

SALMON, R. 1982 The shape of the main thermocline. *J. Phys. Oceanogr.* **12**, 1458–1479.

SALMON, R. 1998 *Lectures on Geophysical Fluid Dynamics*. Oxford University Press.

SAWYER, J. S. 1949 The significance of dynamic instability in atmospheric motions. *Q. J. R. Meteorol. Soc.* **75**, 364–374.

STEPHENS, J. C. & MARSHALL, D. P. 2000 Dynamical pathways of Antarctic bottom water in the Atlantic. *J. Phys. Oceanogr.* **30**, 622–640.

STEWART, A. L. & DELLAR, P. J. 2010 Multilayer shallow water equations with complete Coriolis force. Part 1. Derivation on a non-traditional beta-plane. *J. Fluid Mech.* **651**, 387–413.

STEWART, A. L. & DELLAR, P. J. 2011*a* Cross-equatorial flow through an abyssal channel under the complete Coriolis force: Two-dimensional solutions. *Ocean Model.* **40**, 87–104.

STEWART, A. L. & DELLAR, P. J. 2011*b* The rôle of the complete Coriolis force in cross-equatorial flow of abyssal ocean currents. *Ocean Model.* **38**, 187–202.

STEWART, A. L. & DELLAR, P. J. 2012*a* Cross-equatorial channel flow with zero potential vorticity under the complete Coriolis force. *IMA J. Appl. Math.* **77**, 626–651.

STEWART, A. L. & DELLAR, P. J. 2012*b* Multilayer shallow water equations with complete Coriolis force. Part 2. Linear plane waves. *J. Fluid Mech.* **690**, 16–50.

STONE, P. H. 1966 On non-geostrophic baroclinic stability. *J. Atmos. Sci.* **23**, 390–400.

STONE, P. H. 1971 Baroclinic stability under non-hydrostatic conditions. *J. Fluid Mech.* **45**, 659–671.

STRANG, G. 1966 Necessary and insufficient conditions for well-posed Cauchy problems. *J. Differ. Equations* **2**, 107–114.

SUN, W. Y. 1995 Unsymmetrical symmetrical instability. *Q. J. R. Meteorol. Soc.* **121**, 419–431.

TAYLOR, G. I. 1931 Effect of variation in density on the stability of superposed streams of fluid. *Proc. R. Soc. Lond. A* **132**, 499–523.

THUBURN, J., WOOD, N. & STANIFORTH, A. 2002 Normal modes of deep atmospheres. I: Spherical geometry. *Quart. J. Roy. Meteorol. Soc.* **128**, 1771–1792.

VALLIS, G. K. 2006 *Atmospheric and Oceanic Fluid Dynamics*. Cambridge University Press.

WANG, F. & QI, L. 2005 Comments on "Explicit criterion for the positive definiteness of a general quartic form". *IEEE Trans. Autom. Control* **50**, 416–418.

WHITE, A. A. 2002 A view of the equations of meteorological dynamics and various approximations. In *Large-Scale Atmosphere-Ocean Dynamics 1: Analytical Methods and Numerical Models* (ed. J. Norbury & I. Roulstone), pp. 1–100. Cambridge University Press.

WHITE, A. A. & BROMLEY, R. A. 1995 Dynamically consistent, quasi-hydrostatic equations for global models with a complete representation of the Coriolis force. *Q. J. R. Meteorol. Soc.* **121**, 399–418.

WHITHAM, G. B. 1974 *Linear and Nonlinear Waves*. Wiley Interscience.

XUI, Q. & CLARK, J. H. E. 1985 The nature of symmetric instability and its similarity to convective and inertial instability. *J. Atmos. Sci.* **42**, 2880–2883.